AMES LABORATORY

Iowa State University

Ames, Iowa

EFFECT OF MASS TRANSFER ON THE MOTION

OF A LIQUID-LIQUID INTERFACE

by

William Allen Scholle

Ph.D. Thesis, February 1970

DISCLAIMER

This report was prepared as an account of work sponsored by an agency of the United States Government. Neither the United States Government nor any agency Thereof, nor any of their employees, makes any warranty, express or implied, or assumes any legal liability or responsibility for the accuracy, completeness, or usefulness of any information, apparatus, product, or process disclosed, or represents that its use would not infringe privately owned rights. Reference herein to any specific commercial product, process, or service by trade name, trademark, manufacturer, or otherwise does not necessarily constitute or imply its endorsement, recommendation, or favoring by the United States Government or any agency thereof. The views and opinions of authors expressed herein do not necessarily state or reflect those of the United States Government or any agency thereof.

DISCLAIMER

Portions of this document may be illegible in electronic image products. Images are produced from the best available original document.

EFFECT OF MASS TRANSFER ON THE MOTION

OF A LIQUID-LIQUID INTERFACE

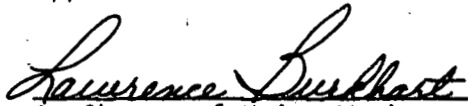, by
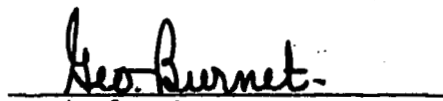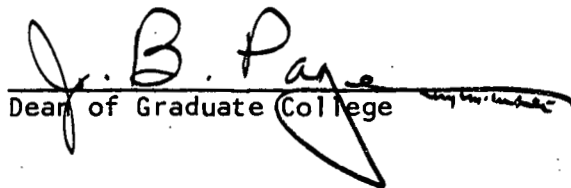
William Allen Scholle

A Dissertation Submitted to the

Graduate Faculty in Partial Fulfillment of

The Requirements for the Degree of

DOCTOR OF PHILOSOPHY

Major Subject: Chemical Engineering

Approved:

In Charge of Major Work

Head of Major Department

Dean of Graduate College

Iowa State University
Of Science and Technology
Ames, Iowa

1970

TABLE OF CONTENTS

ABSTRACT

Pressure changes induced by a change in interfacial tension on the curved interface of a static drop were used to determine the driving force and subsequent motions of the dopplet interface. At any time, the drop was considered static with dynamic pressures imposed on it. These dynamic pressures included the interfacial tension change caused by solute spreading radially from the apex of the drop along the interface and the effect of a wave propagating from the apex.

The interfacial tension change was achieved experimentally by introducing a tiny drop of a cyclohexanol solution to the apex of a cyclohexane or carbon tetrachloride drop which was resting on a flat plate immersed in water. High speed motion pictures of the dynamic drops and of the corresponding motion that occurred in a flat interface were taken. The mathematical model along with the boundary conditions measured from the pictures was used to calculate droplet shapes which compared favorably to actual droplet shapes.

INTRODUCTION

To better understand the mechanism of mass transfer in liquid-liquid systems, a more thorough knowledge of droplet mechanics is necessary, since mass transfer most often occurs when one phase is dispersed in the other in the form of drops. Circulation in the droplet interior carries solute to the interface where it transfers across the interface to the outside liquid. Concentration gradients in the interface create turbulence in the form of spontaneous interfacial movement producing a rapid change in droplet shape and a significant increase in the interfacial area available for mass transfer. Systems which exhibit interfacial turbulence provide higher rates of mass transfer than those without interfacial turbulence.

Visual interfacial turbulence, the formation of small waves at the interface, is caused by a combination of two different effects. The first of these is the Marangoni effect where a change in concentration at the interface causes a surface tension gradient. This gradient produces rapid motion in the plane of the interface; resulting viscous shear stresses transmit this motion to the bulk phases in the immediate vicinity of the interface. If the interface remains planar during this movement, there is no visual turbulence. However, if the interface should become curved when an interfacial tension gradient is imposed, a second effect will cause movement perpendicular to the interface. This secondary effect causes a violent change in the shape of the droplet interface due to the sudden imbalance of pressure across the interface. When the interface is initially flat, the deformation may be in the form of small waves or ripples.

The purpose of this work is to develop a model to describe the change in droplet shape that occurs in conjunction with the Marangoni effect. The model was developed by introducing approximate dynamic pressures, based partly on qualitative observations, into the equations describing a static drop. The dynamic pressures include the effect of a variation of interfacial tension distribution with time and the effect of a wave that propagates from the droplet apex. The droplet profiles predicted by the model were compared to measurements obtained from high speed motion pictures of an actual drop of known initial curvature undergoing motion induced by a prescribed concentration change.

LITERATURE REVIEW

An excellent review of the literature on interfacial dynamics has been given by Scriven and Sternling (19), who cite articles beginning with the first correct description by James Thomson (24) of what has become known as the Marangoni effect, to articles published in 1959. Because Thomson's work went unnoticed for several years and because Marangoni contributed a great deal of qualitative information about surface tension variations, the effect was given his name.

Although motions driven by interfacial tension gradients were known to exist, their importance in mass transfer operations did not become apparent until the early 1950's. Lewis and Pratt (12), working at Britain's Atomic Energy Research Establishment at Harwell, had developed an emperical correlation relating the diameter of drops in packed columns to the surface tension and the densities of the liquids used. The correlation was restricted to systems where the two liquid phases were in mutual equilibrium with a solute. However, in later experiments when the solute was not equilibrated, mass transfer occurred and the actual droplet size was larger than predicted by their earlier correlation. They thought this might have been due to higher interfacial tension, but found that the interfacial tension measured experimentally was not only lower, but also that the drops were disturbed by "rippling" of the surface and "erratic pulsations." Aluminum powder sprinkled on the surface showed that "violent circulation" was taking place. They speculated that this was caused by thermal gradients set up by heats of reaction of the transferring solutes.

Garner, Nutt, and Mohtadi (5) working at the same laboratory,

contributed additional qualitative information by observing that droplet motion depended upon the rate of droplet formation, solute concentration, and nature of the liquids. They also found that small amounts of a surface active compound dissolved in the drop suppressed the pulsating behavior.

Lewis (11) built a two phase mass transfer cell to obtain mass transfer data for testing the two film theory. Using the film theory, he calculated mass transfer coefficients for a single phase using a two component system and developed an empirical correlation for mass transfer coefficients as a function of stirring speed and kinematic viscosity. Using this correlation, he calculated mass transfer rates for three component systems, assuming that resistance to mass transfer at the interface was negligible.

Of thirty-two systems which were used to compare calculated mass transfer rates to experimental mass transfer rates, fifteen were in reasonable agreement, eight were faster, and nine were slower than predicted. All eight systems that had high mass transfer coefficients also exhibited marked interfacial turbulence. One of his conclusions was that the film theory should not be used to correlate mass transfer data in systems where interfacial turbulence is present.

Sherwood and Wei (20), using an apparatus similar to that of Lewis, planned to obtain liquid-liquid extraction data that could test the validity of the film and penetration theories of mass transfer. Systems were chosen in which a chemical reaction would occur and in which the kinetics of the reaction were known because they wanted to find the effect of ion movement as opposed to the diffusion of molecules. Their data

gave much higher overall mass transfer coefficients than the film theory
could account for and the following possible causes were listed:

(1) faster ion diffusion

(2) concentration effect on distribution coefficient

(3) temperature change due to chemical reaction

(4) interfacial turbulence.

They concluded, for their system, that interfacial turbulence was an im-
portant factor in determining mass transfer rates and proceeded to observe
interfacial motion for several other systems. In almost every case there
was rippling of the surface and a tendency toward spontaneous emulsifi-
cation.

Zuiderweg and Harmens (26) found interfacial effects in distillation
of binary systems in various types of equipment. Interfacial tension
variations seemed to have a significant effect on the contact area between
the liquid and gas phases and also on the mass transfer rates, especially
in equipment where bubbles or drops were involved. They suggested that
surface tension variations have a greater effect than density, viscosity,
or diffusivity variations.

Haydon (7) injected acetone toward pendant water drops immersed in
toluene and noticed that they "kicked" violently in the direction of the
capillary from which the acetone was introduced. Similar results were
found for an air bubble in toluene.

In a related experiment, when a water drop was immersed in a uniform
solution of acetone in toluene, the water drop oscillated erratically.
However, when an air bubble was used in place of the water drop, there

were no signs of movement. Since the amount of acetone transferred to the air bubble was negligible, there was no local concentration change at the interface of the air bubble. Thus, he concluded that an essential condition for oscillation was a non-uniform solute distribution around the drop.

Haydon and Davies (8) continued the investigation with a more quantitative approach. For a model they used spherical pendant drops that would move as a pendulum rather than deform under the influence of mass transfer. They modified Laplace's equation to include the effect of an interfacial tension change over the area influenced by the concentration fluctuation at the interface. The modified equation was $P_i - P_o = 2(\sigma - \Delta\sigma)/r$. The $\Delta\sigma$ term is equivalent to increasing the pressure inside the drop, thus causing the drop to kick in the direction observed experimentally. They also noted the possibility of a change in curvature in addition to a "kick" but this was not observed experimentally.

An expression was derived to calculate the maximum energy that could be instanteously imparted to a unit area of the drop due to a known change in interfacial tension. They assumed that all this energy was dissipated during subsequent oscillations of the pendant drop. This energy dissipation was mathematically described by assuming that the drop behaved as a sphere moving through a viscous fluid. From the resulting mathematical expression along with droplet velocity and displacement measurements, the energy dissipation due to viscosity was calculated. Then the energy imparted to the drop was compared to the energy dissipated and they agreed to the extent that the basic assumptions in their calculations were

confirmed.

In an experimental apparatus devised by Pétré and Schayer-Polischuk (15) two liquid drops were connected by a tube so that the average pressure was the same in both drops. They were both placed in a chamber filled with liquid, but the chamber was divided by a partition. A solute was then added to that part of the system containing only one of the drops. The corresponding pressure change affected the size of the other drop without disturbing its interfacial tension. At equilibrium the curvatures of two such drops are related by $\sigma_A/\sigma_B = R_A/R_B$.

Of special interest in this work were the conditions that caused an instability where one of the drops broke away. Measurements were made so that the ratio of the curvatures could be plotted against the ratio of the heights of the two drops. When the projected equilibrium for a prescribed interfacial tension change represented a point on the plot where the slope was positive, the system was unstable. Physically, this represented the condition where the radius of curvature was less than the radius of the tube connecting the drops. This type of equipment might also be useful in isolating the effect of a concentration change on the interfacial pressure drop.

With a qualitative picture of interfacial turbulence in mind, Sternling and Scriven (21) analyzed the problem mathematically to predict what conditions were necessary for interfacial turbulence to occur. They considered a flat, semi-infinite interface with two dimensional disturbances. The diffusion equation, along with linearized equations of motion, enabled them to solve for a dimensionless wave number and a dimensionless growth

constant. The signs of these numbers, which are functions of physical constants, determine stability or instability. The importance of their work is that they have shown that interfacial turbulence is a result of hydrodynamic instability which creates conditions required for the Marangoni effect.

Orell and Westwater (13) tried to verify experimentally the theory of Sternling and Scriven. They used a Schlieren apparatus to view a liquid-liquid interface under the influence of mass transfer and reasoned that the same types of cellular patterns that develop at the interface in thermal instability should also appear during interfacial mass transfer. These are the patterns viewed by Bénard when he spread small particles on the surface of a liquid heated from below. Rayleigh (16) explained these patterns mathematically on the basis of hydrodynamic instability due to density variations. (Recently it has been shown that Bénard's hexagonal cells were also a result of surface tension variations (2, 14)).

As expected, Orell and Westwater found that ploygonal cells having from three to seven sides formed at the interface. They also encountered stripes--elongated bands lying parallel to each other and slowly propagating across the interface. Stripes did not occur until the interfacial contact had exceeded fifteen hours. They also noticed ripples confined by cell or stripe boundaries.

They measured the cell diameters, which are equivalent to the wave lengths described by Sternling and Scriven. The wave lengths calculated from the theory were approximately an order of magnitude smaller than those found experimentally and observed phenomena was concluded to be much more

complex than the present theory suggests.

Sawistowski and Goltz (17) also used a Schlieren arrangement to determine the onset of interfacial turbulence. Their interface was that of a drop formed and withdrawn by the same nozzle. They correlated the mass transfer coefficient for cases of visual and non-visual turbulence and found that in the turbulent regime, the rate of mass transfer was a function of the solute concentration and increased almost linearly with the equilibrium interfacial tension changes that might occur due to concentration changes.

In a short communication, Ellis and Biddulph (3) discussed the mechanism for wave formation on a flat interface. They said that the interaction between the surface tension variation and the rate of surface movement in the plane of the inteface sets up bulk phase motions which tend to move the interface when the interface is most vulnerable to a change in shape.

Valentine, Sather, and Heideger (25) presented a more quantitative analysis of the motion of an interface. They coalesced a free stream drop with a small drop of surface active material and observed the resultant changes in shape. They calculated the internal energy change due to displacement, wave motion, and oscillation, and let the remainder be due to "unassigned circulatory flow." They found that 19 to 61 percent of the total energy dissipation was accounted for by motions other than "unassigned circulatory flow." Further developing a treatment by Lamb on oscillating liquid spheres for two liquid phases, they compared calculated values for oscillation frequency and amplitude decay constant to

those obtained experimentally. The calculated frequencies agreed within 35 percent but the decay constants were nearly an order of magnitude too high. The assumptions used in the development were very limiting, however, and large errors were not unexpected.

Most recently, Suciu, Smigelschi, and Ruckenstein (23) studied the phenomenon of spreading of thin, soluble, surface films. They fed solute onto a surface, allowing it to spread radially at steady state and observing the resulting flow patterns with a Schlieren apparatus. They used several systems and reported qualitatively the results in terms of wave formation and the type of film formation.

In a more recent article (22) the same authors reported on continued work with the same experimental apparatus, but in addition, a photographic system had been devised to measure film velocities as a function of radius. The contact angle of the film with the bulk liquid was measured and found to be smaller than for equilibrium contact of the same two liquids. This difference was attributed to what was called dynamic values of interfacial tension which were different from those obtained in static interfacial tension measurements and to surface velocities which produced forces that must be balanced by interfacial tension forces.

STATIC DROPS

This section provides the background for understanding the mathematical description of three forms of static drops:

1) a drop in static equilibrium resting on a flat surface

2) a hypothetical static drop with a non-uniform interfacial tension

3) a drop having an upward force applied in the region of the apex. All of the drops will be considered surfaces of revolution and will be affected only by forces which are symmetrical with respect to the axis of revolution. The principles formulated here will be extended and applied later in the description of dynamic drops.

Drop Resting on a Solid Surface

In general, the shape of any liquid-liquid interface of uniform interfacial tension may be described by the equation of Young and Laplace,

$$\Delta P = \sigma \left(\frac{1}{R_1} + \frac{1}{R_2} \right) \tag{1}$$

The interfacial tension, σ, is a physical constant for a given static system. To calculate the coordinates of the interface, a functional relationship is necessary to relate ΔP, the pressure drop across the interface and the two radii of curvature, R_1 and R_2, in terms of the coordinates. Bashforth and Adams (1) present the equations and show how a Runge-Kutta integration may be used to solve for the interfacial coordinates.

They located the origin of their coordinate system at the apex of the drop as in Figure 1. The pressure drop at any point is the pressure
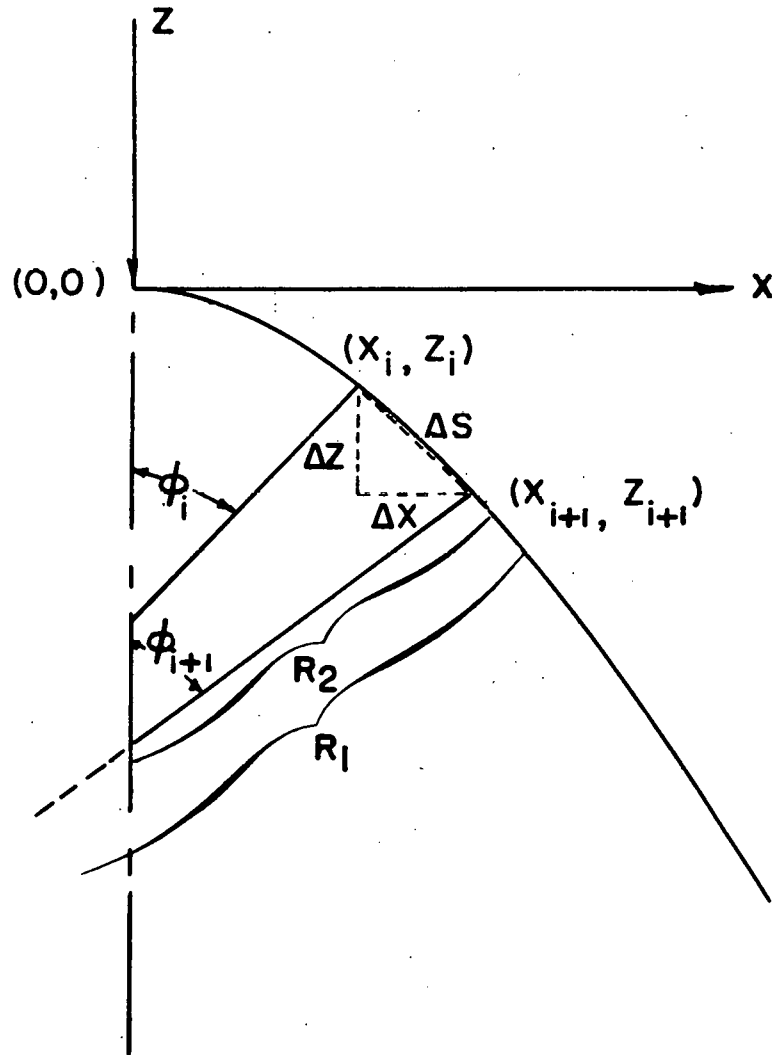
Figure 1. Droplet geometry for a surface of revolution.

drop at the origin plus the pressure drop due to hydrostatic head,

$$\Delta P = \Delta P_o + (\rho_d - \rho_c)gz = \sigma\left(\frac{1}{R_1} + \frac{1}{R_2}\right) \tag{2}$$

However, at the origin ($z = 0$), R_1 and R_2 are equal for a surface of revolution and their common value is set equal to b, the radius of curvature at the origin. Equation (2) now becomes

$$\Delta P_o = 2\sigma/b \tag{3}$$

and substituting this result back into (2) gives

$$2\sigma/b + (\rho_d - \rho_c)gz = \sigma\left(\frac{1}{R_1} + \frac{1}{R_2}\right) \tag{4}$$

The geometry of the surface provides the relations:

$$\frac{1}{R_1} = \frac{d\Phi}{ds} \; , \tag{5}$$

$$\frac{1}{R_2} = \frac{\sin\Phi}{x} \; , \tag{6}$$

$$\frac{dx}{ds} = \cos\Phi \text{, and} \tag{7}$$

$$\frac{dz}{ds} = \sin\Phi \; . \tag{8}$$

Substituting the equality in (6) for R_2 and solving for $1/R_1$, in Equations (4) and (5) yields

$$\frac{d\Phi}{ds} = -\frac{\sin\Phi}{x} + \frac{\Delta\rho\, gz}{\sigma} + \frac{2}{b} \; . \tag{9}$$

Now there are three differential equations (7), (8), and (9) in terms of the dependent variables x, z, and ϕ and the dependent variable, s. These equations may be integrated numerically for given values of the parameter, b, whose value for a given drop is uniquely determined when the boundary conditions are satisfied.

Suppose the volume of the drop and its angle of contact with a solid surface at its base are known. These are the boundary conditions in the sense that the numerical integration is terminated when ϕ reaches a prescribed value; then the volume under the surface of revolution defined by the solution to the three differential equations is calculated. The value of b is corrected and the equation solved again until the contact angle is satisfied and simultaneously the calculated volume agrees with the known droplet volume.

Drop with Non-uniform Interfacial Tension

This procedure can also be used to consider the shape a drop with a non-uniform interfacial tension would assume if it were possible for such a drop to exist in a static condition. In the strictest sense, an interfacial tension gradient can only exist when velocity gradients at the interface produce stresses which tend to balance the interfacial imbalance (Landau and Lifschitz (10)). However, once an interfacial tension gradient is established, it may be balanced to some extent by an alteration in curvature. To determine the equilibrium shape tendency of a drop under these conditions a limiting case is considered where the imbalance of interfacial tension forces is completely balanced by a change in

curvature and hydrostatic head. Equation (1) is no longer valid under this hypothesis and a new development must be considered.

Let $\overline{\Delta P}$ be the average pressure drop across the element of interface described by revolving Δs in Figure 1. The vertical force resulting from the pressure drop is $\overline{\Delta P}\ 2\pi x\ \Delta x$. This force must balance the vertical component of the surface tension forces,

$$- 2\pi x \sigma\ \sin\ \Phi + 2\pi (x + \Delta x)(\sigma + \Delta\sigma)\ \sin\ (\Phi + \Delta\Phi) \tag{10}$$

where
$$\Delta x = x_{i+1} - x_i\ ,$$

$$\Delta\sigma = \sigma_{i+1} - \sigma_i, \text{ and}$$

$$\Delta\Phi = \Phi_{i+1} - \Phi_i\quad .$$

Equating these two opposing forces, dividing by Δx and taking the limit as Δx approaches zero gives

$$\Delta P\ 2\pi x = 2\pi x\ \cos\ \Phi\ \frac{d\Phi}{dx} + 2\pi\sigma\ \sin\ \Phi + 2\pi x\ \frac{d\sigma}{dx}\ \sin\ \Phi \tag{11}$$

Dividing by $2\pi x$ and employing Equations (5) through (8) to eliminate x gives

$$\Delta P = \sigma\ (\frac{1}{R_1} + \frac{1}{R_2}) + \tan\ \Phi\ \frac{d\sigma}{ds} \tag{12}$$

which will be used in place of Equation (1).

Experiments involving the application of solute at the apex of a drop show that both positive- and negative-beta drops move upward when $d\sigma/ds$ is positive in the region of the apex. (The sign of beta is determined by the sign of the density difference, $\rho_d - \rho_c$.) Linear forms of $\sigma(s)$ over the portion of the drop near the apex were chosen to simulate the contact of solute. The interfacial tension distributions in Figure 2 were used to
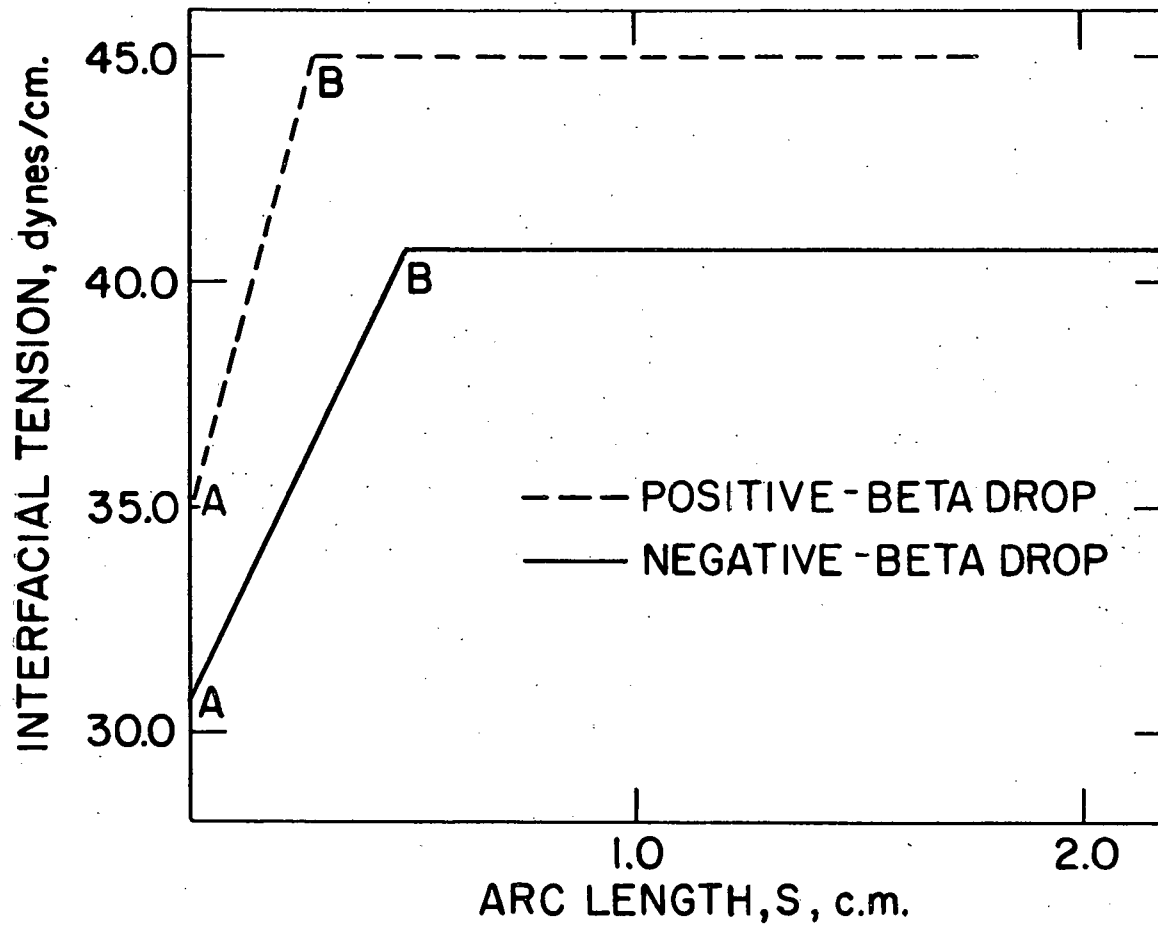
Figure 2. Hypothetical interfacial tension distribution over droplet surface.

calculate the droplet shapes in Figures 3 and 4. Both sets of drops are compared on the basis of same volume and contact angle. These theoretical equilibrium shapes are in accord with the movement of actual drops whose initial movements must be toward a new equilibrium shape.

The negative-beta drops in Figure 3 show the profile of the drop with non-uniform interfacial tension to lie between the profiles of drops with uniform interfacial tension. This might be expected since the profile should approach that of the static drop with an interfacial tension of 30.7 dynes/cm. as $d\sigma/ds$ becomes smaller and the gradient covers a larger portion of the interface.

For the positive-beta system, the profile of the drop with non-uniform interfacial tension does not lie between the other two profiles. From a static point of view, this result is unexpected, but the new shape agrees with the dynamic tendency. Unfortunately, the analysis may not be tested by allowing an interfacial tension gradient to exist over the entire drop since Equation (12) becomes unbounded at $\Phi = \pi/2$. At $\Phi = \pi/2$, the vertical force contribution from the pressure drop is zero and only shear stresses may balance the forces. This is in complete opposition to the limiting condition being analyzed.

Drop with an External Force

The shape of a drop acted on by an external vertical force is also of interest. The magnitude of the vertical force will be,

$$F = \int_{A_h} \Delta P dA$$

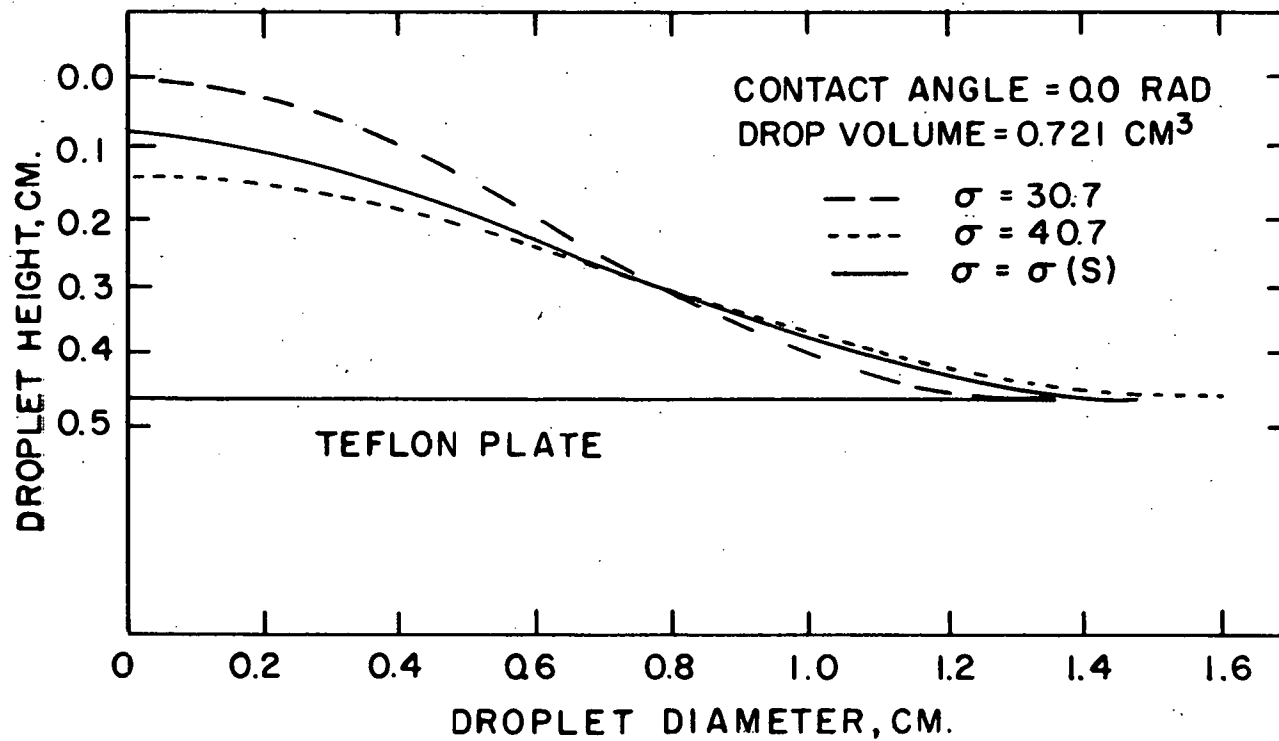where F is the magnitude of the inherent force exerted by the portion of

Figure 3. Comparison of a static drop of non-uniform interfacial tension to static drops of uniform interfacial tension for negative-beta system.
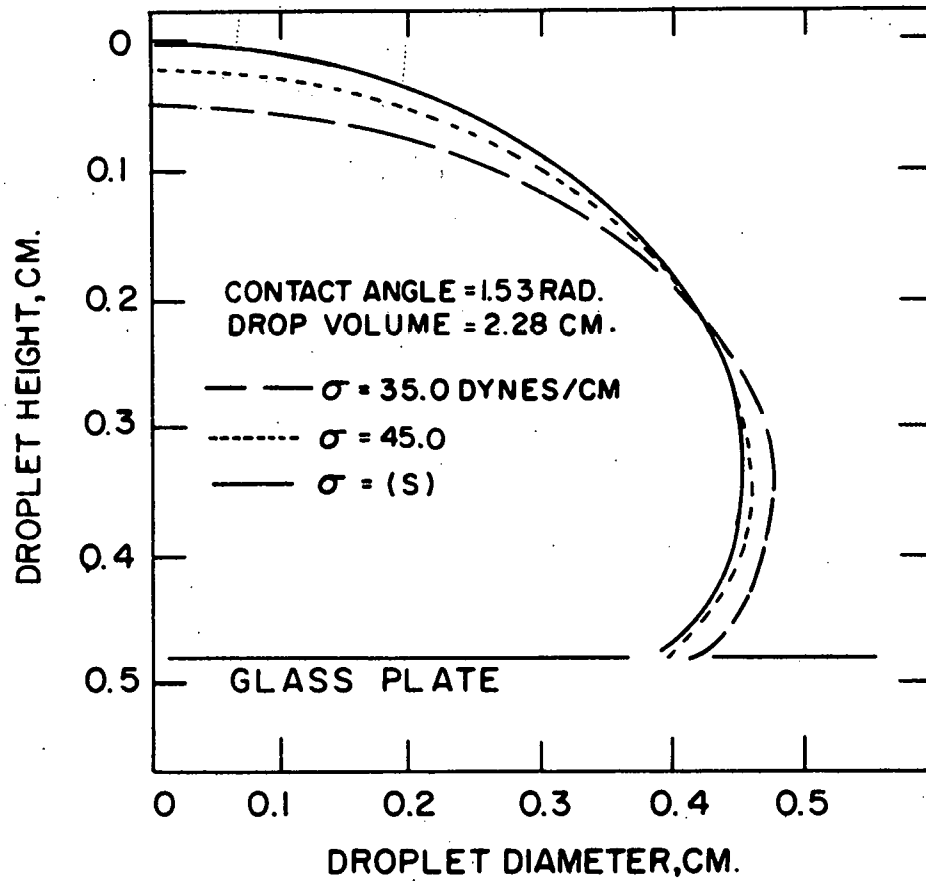
Figure 4. Comparison of a static drop of non-uniform interfacial tension
to static drops of uniform interfacial tension for positive-
beta system.

the drop from the origin to some arbitrary height, h. This integral can be evaluated to give a relationship necessary for the solution of the necessary differential equations.

As given by Eskinazi (4) the force on a body immersed in another fluid is

$$- \vec{F} = -\int_S \vec{n}\, P_o dS + \int_V \rho_d \vec{g} dV$$

where the first term on the right is the buoyant force and the second term is the weight of the drop. Substituting for P_o in the first integral and applying the divergence theorem in the second integral, gives,

$$- \vec{F} = -\int_S \vec{n}(\dot{P}_{o_o} + \rho_c gz)dS + \int_V \vec{\nabla}\,(P_{o_i} + \rho_d gz)dV$$

$$= -\int_S \vec{n}(\dot{P}_{o_o} + \rho_c gz)dS + \int_S \vec{n}(P_{o_i} + \rho_d gz)dS$$

The combination of the two integrals produces,

$$\vec{F} = \int (\dot{P}_{o_o} - \dot{P}_{o_i} + \Delta\rho gz)\, \vec{n}dS \quad .$$

The term in parentheses is equivalent to ΔP and the only area component that contributes to the force is the vertical component so the above equation may be written in terms of the magnitude of the vertical force,

$$F = \int \Delta P \, dA \quad .$$

This establishes the result in Equation (13) which may be integrated for a drop by substituting Equation (1) for ΔP:

$$F = \int_A \sigma(\frac{1}{R_1} + \frac{1}{R_2})dA = \int_0^{x_h} \sigma(\frac{1}{R_1} + \frac{1}{R_2}) \, 2\pi x \, dx$$

$$= 2\pi\sigma \int_0^{x_h} (\frac{d\Phi}{dx} \, \frac{dx}{ds} + \frac{\sin \Phi}{x}) \, x \, dx = 2\pi\sigma \int_0^{x_h} x \cos \Phi \, d\Phi + \sin \Phi \, dx$$

$$= \int_0^{x_h} d(2\pi x \sigma \sin \Phi) = 2\pi x_h \sigma \sin \Phi_h$$

Therefore, the vertical force on any static drop at an arbitrary height, $z = h$, is

$$F = 2\pi x_h \sigma \sin \Phi_h \quad . \tag{14}$$

Suppose a drop is acted upon by a vertical external force, F_e, exerted by a glass tube of radius x_o as in Figure 5. At equilibrium the total force at any point, $z = h$, is

$$F_T = \int_0^{x_h} \sigma(\frac{1}{R_1} + \frac{1}{R_2}) \, 2\pi x dx = F_e + F$$

$$= \int_0^{x_o} \sigma(\frac{1}{R_{10}} + \frac{1}{R_{20}}) \, 2\pi x dx + \int_{x_o}^{x_h} \sigma(\frac{1}{R_1} + \frac{1}{R_2}) \, 2\pi x dx$$

$$F_T = A_o\sigma(\frac{1}{R_{10}} + \frac{1}{R_{20}}) + 2\pi\sigma [x_h \sin \Phi_h - x_o \sin \Phi_o] \tag{15}$$

The first term on the right side of Equation (15) represents the magnitude of the external force,
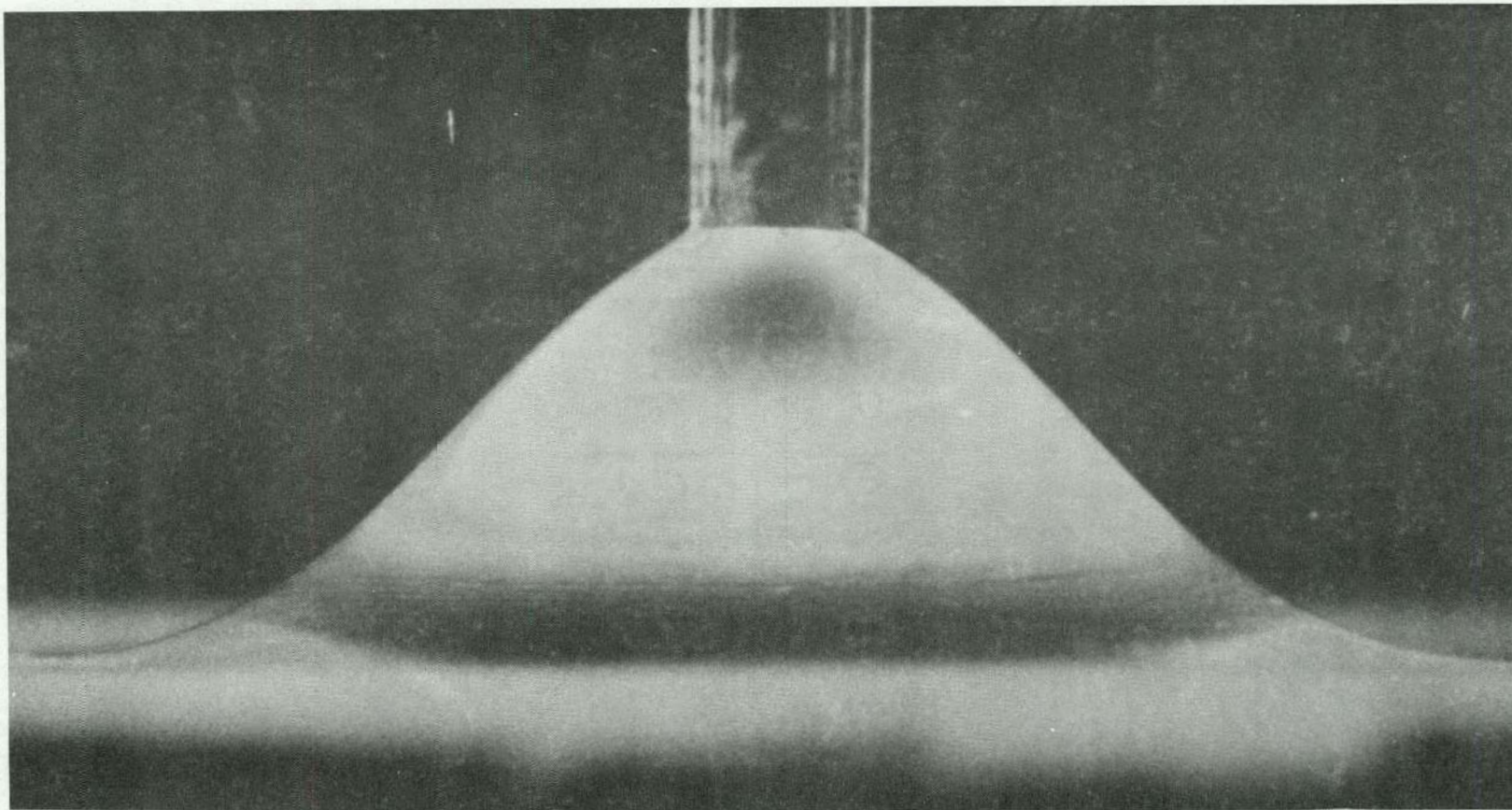
Figure 5. Negative-beta drop with an upward force exerted by a round glass tube.

$$F_e = A_o \sigma \left(\frac{1}{R_{10}} + \frac{1}{R_{20}} \right) = A_o \Delta P_o \tag{16}$$

If F_e and x_o were measured, the coordinates of the profile could be calculated directly. F_e is distributed over the area, A_o, where A_o is given by

$$A_o = \pi x_o^2 \tag{17}$$

for a round glass tube. The pressure drop at $z = 0$ is

$$\Delta P_o = F_e / A_o \tag{18}$$

The relationship in Equation (14) permits calculation of Φ_o by

$$\Phi_o = \sin^{-1} (F_e / 2\pi x_o \sigma) \quad . \tag{19}$$

Knowledge of the parameter, b, is now unnecessary since ΔP_o is known and Equation (9) becomes

$$\frac{d\Phi}{ds} = - \frac{\sin \Phi}{x} + \frac{\Delta \rho \ gz}{\sigma} + \frac{\Delta P_o}{\sigma} \tag{20}$$

which can be solved along with Equations (7) and (8), as before, with the initial conditions,

1) $z = 0$

2) $x = x_o$

3) $\Phi = \Phi_o$

and a single boundary condition such as droplet volume, contact angle, droplet height, or base diameter.

The force F_e is difficult to measure, particularly in a dynamic drop, but the development can be extended to calculate the magnitude of the force if the radius of the glass tube which applies the force is known. The initial angle, ϕ_o, cannot be calculated from Equation (19) since F_e is unknown and like b, ϕ_o is difficult to measure accurately. So, in solving Equations (4), (5), and (20), ϕ_o will be a parameter that must be determined by a boundary condition. Suppose the two boundary conditions measured from the drop restrict the drop to a known volume and contact angle.

The calculations proceed as follows. An approximate value for ϕ_o is chosen and ΔP_o is calculated by Equations (14) and (18). Now Equations (4), (5), and (20) may be integrated until the known contact angle is reached. The volume calculated for the resulting drop may not agree with the known volume and a new value of ϕ_o is chosen and the iteration continued until a value of ϕ_o is found such that both conditions are satisfied. Not only can the external force be calculated by

$$F_e = \pi \, x_o^2 \, \Delta P_o,$$

but the shape of the drop will also have been determined.

Essentially, the knowledge of the magnitude of F_e has been traded for the knowledge of another boundary condition. If one were given a picture of a static drop with an external force applied, the magnitude of that force could be determined by measuring x_o, a representation of the distribution of F_e. Figure 6 shows such a drop where F_e was determined to be 5.45 dynes exerted by the glass tube.
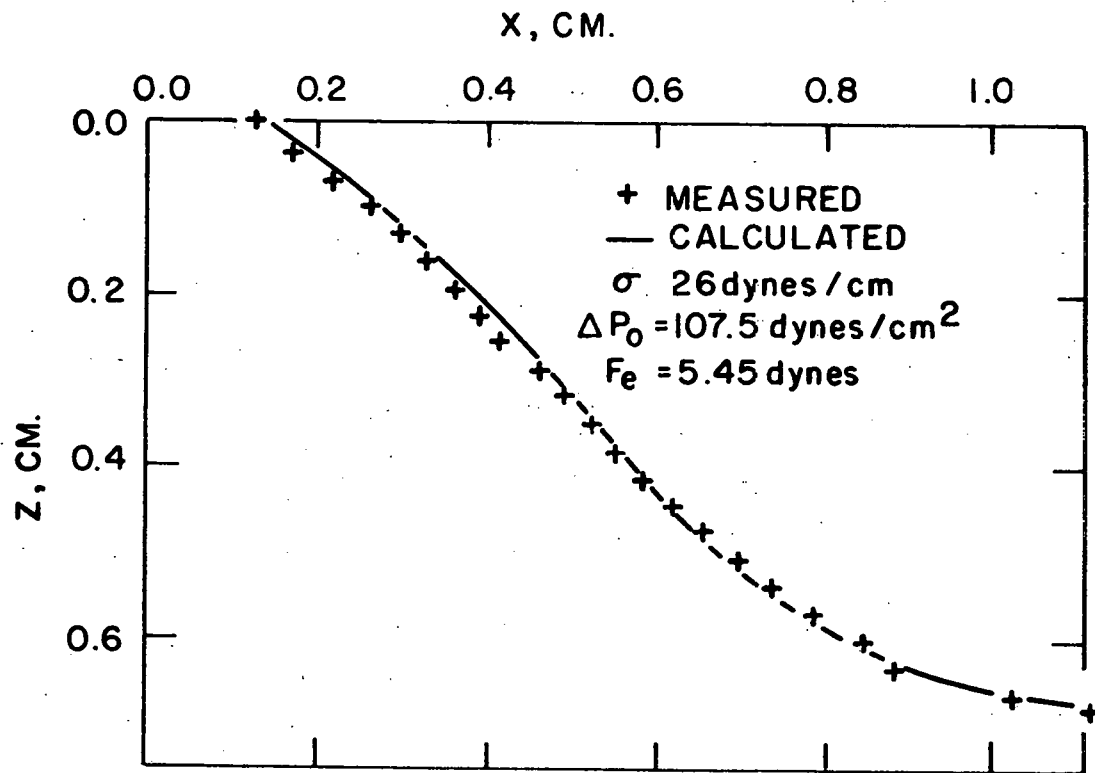
Figure 6. Comparison of measured and calculated profiles of static drop with an external force.

DYNAMIC DROPS

When a solute is injected exactly at the apex of a drop, it spreads symmetrically over the surface so that the interfacial tension may be considered to be a function of arc length, time, and solute concentration. An increase in solute concentration at the interface lowers the interfacial tension and this interfacial tension change causes the droplet interface to move suddenly. The direction in which the interface moves and hence the sign of the velocity vector is related to the sign of the curvature of the drop. The radius of curvature is positive when it is inside the drop and negative when outside the drop. The curvature has the same sign as the radius of curvature. The total curvature is the sum of the reciprocals of the two radii of curvature.

Qualitative Observations

Experimentally, one finds that the direction of movement of the apex is upward when solute meets the interface at the apex. The change in shape for a negative-beta drop is shown in Figure 7 and this is in agreement with the equilibrium tendency, Figure 3. Similarly a positive-beta drop, shown in Figure 8, also rises under the same conditions, supporting the equilibrium tendency as shown in Figure 4.

The curvature is negative near the base of the negative-beta drop shown in Figure 9a. If solute is added at this point of negative curvature the motion is inward, or in other words, the velocity is negative. Figure 10a shows a positive-beta drop pulled up by a glass tube. Solute has just been added to the region of negative curvature near the glass
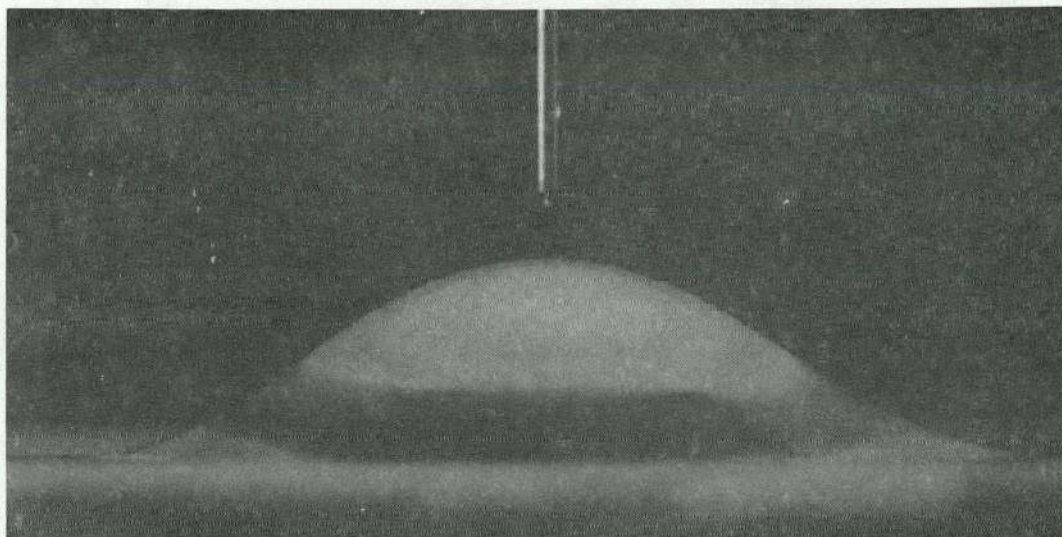
(7a)
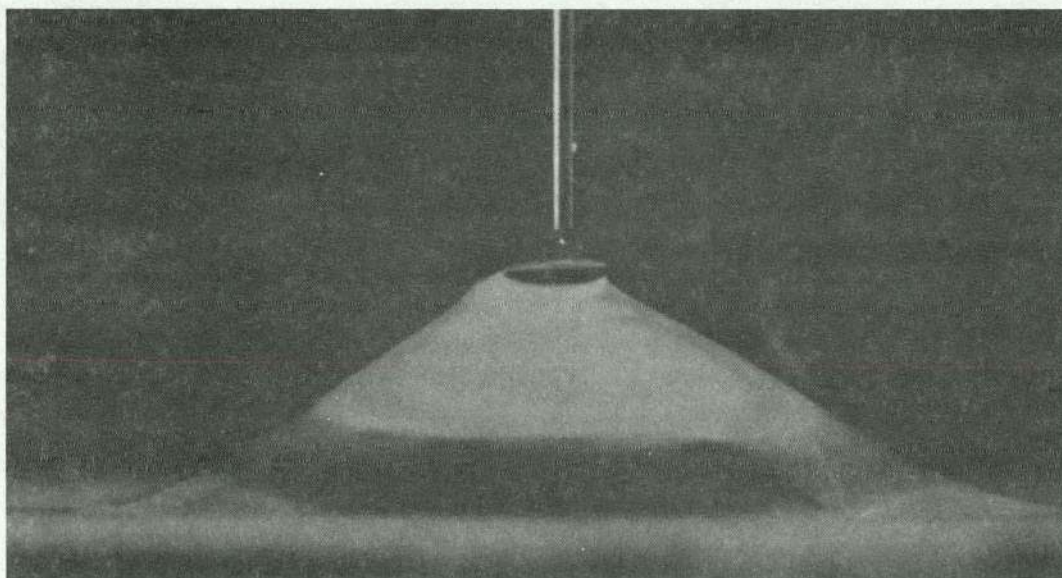
(7b)

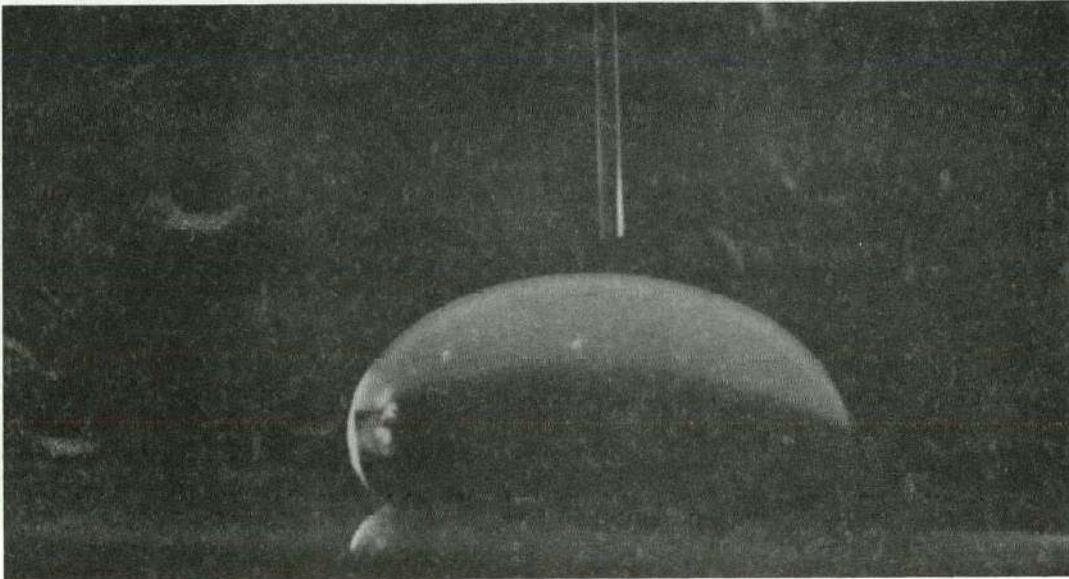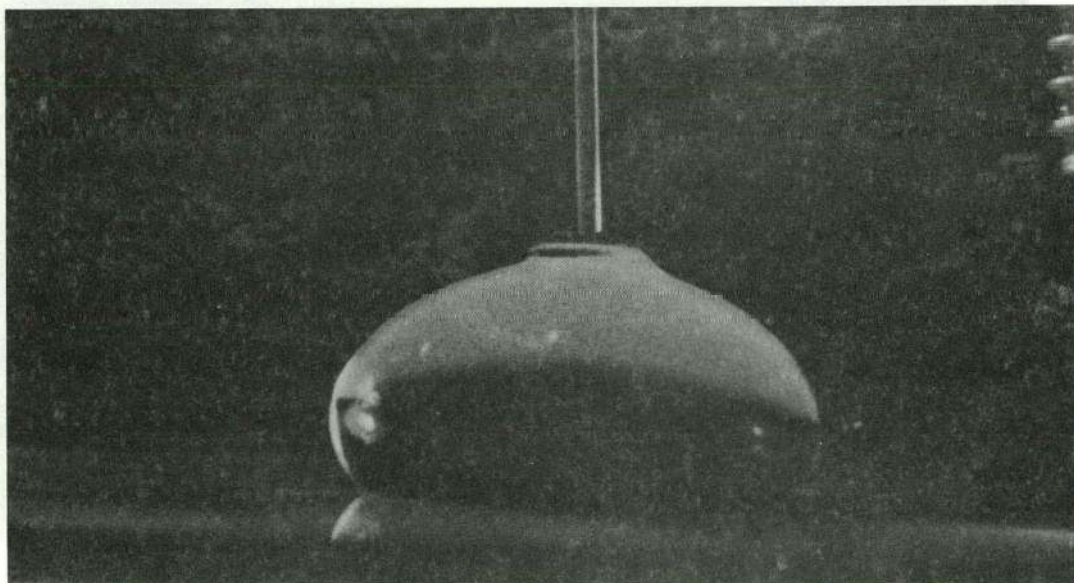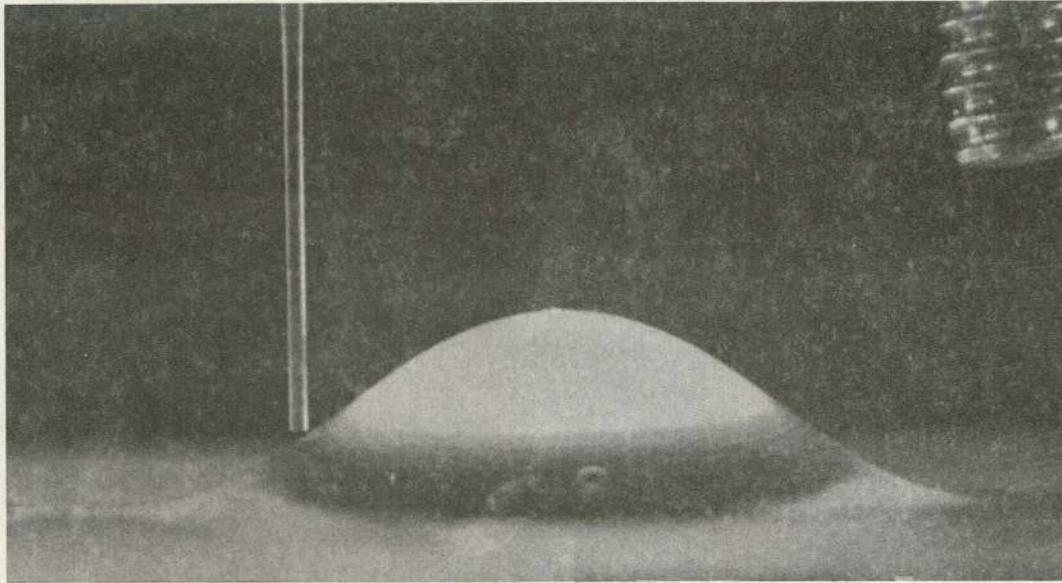Figure 7. Motion of negative-beta drop under the influence of solute at its apex.
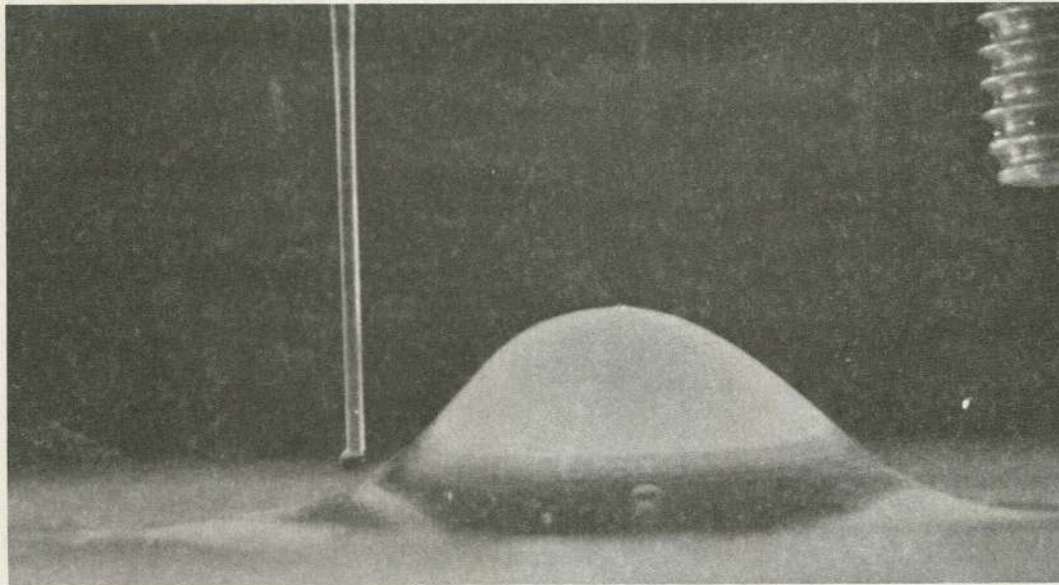
(8a)

(8b)

Figure 8. Motion of positive-beta drop under the influence of solute at its apex.
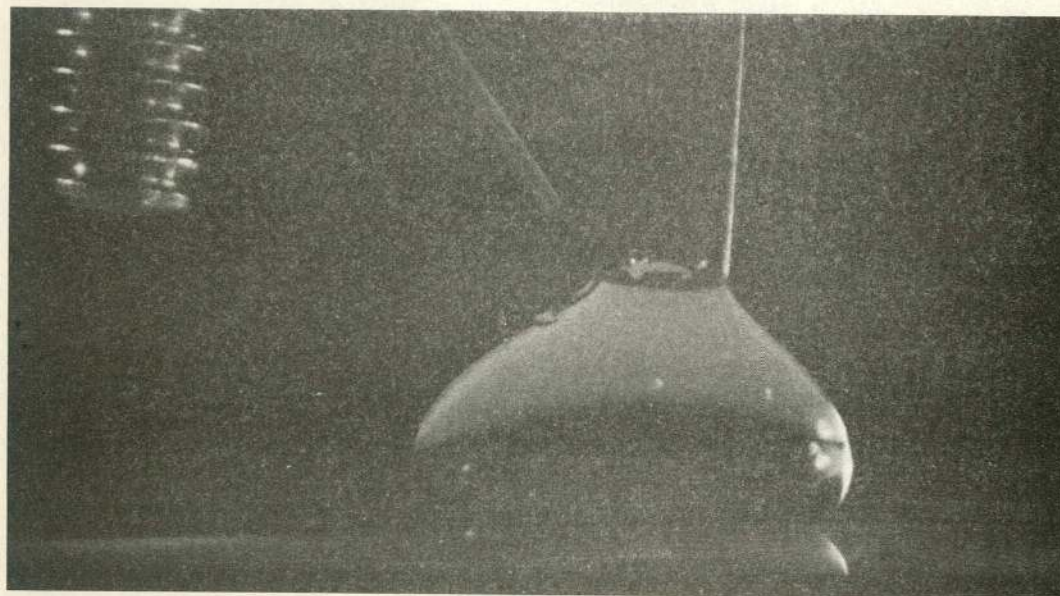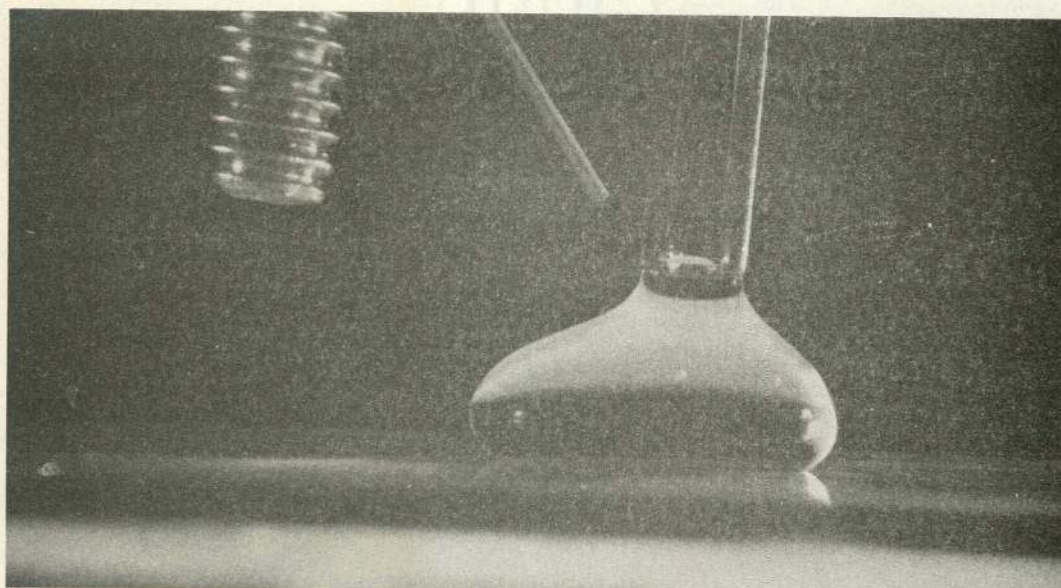
(9a)

(9b)

Figure 9. Motion of negative-beta drop when curvature is negative at point of solute contact.

(10a)

(10b)

Figure 10.   Motion of a positive-beta drop being held by a glass
tube with solute touching at a point of negative
curvature.

tube and the initial motion is inward, but as solute spreads down the interface where the curvature is positive, the motion is in the opposite direction as shown in Figure 10b. The application of equal amounts of solute at two different portions of the same drop is shown in Figure 11. The magnitude of the horizontal movement in 11b is large compared to the vertical movement in 8b shown again on the same page. As before, the velocity is positive and the magnitude of displacement is greater for larger curvature. However, the difference in interfacial displacement in the two pictures is too large to be completely determined by difference in curvature. The resistance to movement caused by hydrostatic head changes must be a resistance factor in Figure 8b.

In summary, these photographs illustrate the following points:

1) the direction of interfacial movement is in the direction of the radii of curvature,

2) the magnitude of the movement is proportional to the magnitude of the initial curvature,

3) changes in hydrostatic pressure alter the pressure drop and subsequent motion.

Items 2 and 3 are interrelated since the initial curvature is partly determined by hydrostatic pressure.

Model Development

The following model applies to an initially static drop and its subsequent motion when dynamic pressures are imposed upon it. From the static drops, initial conditions such as interfacial tension, volume, denisities, base diameter, contact angle, and the coordinates of the interface as well
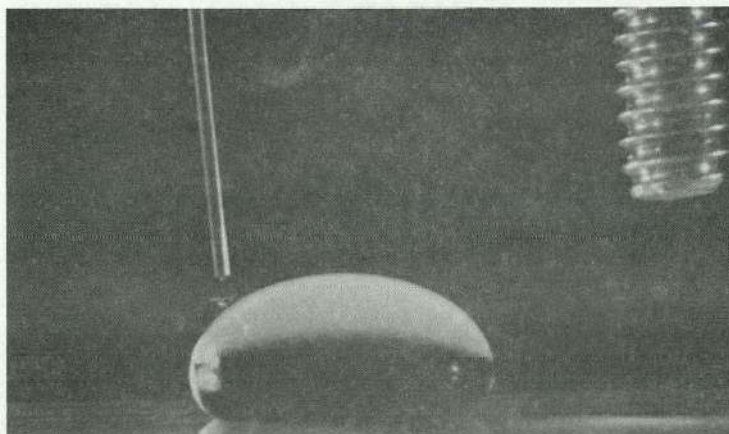
(11a)
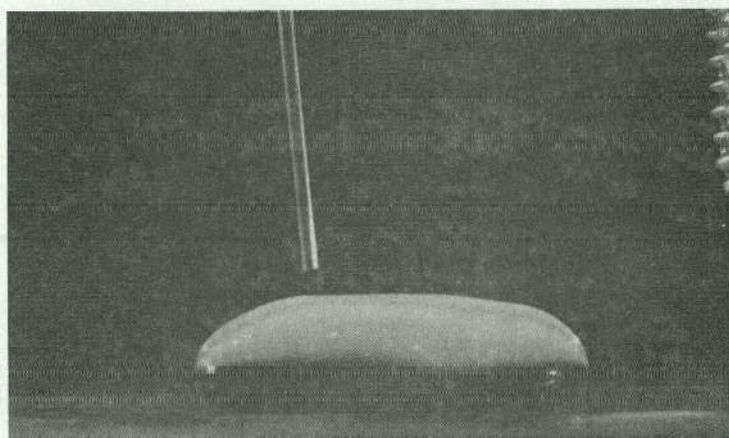
(11b)
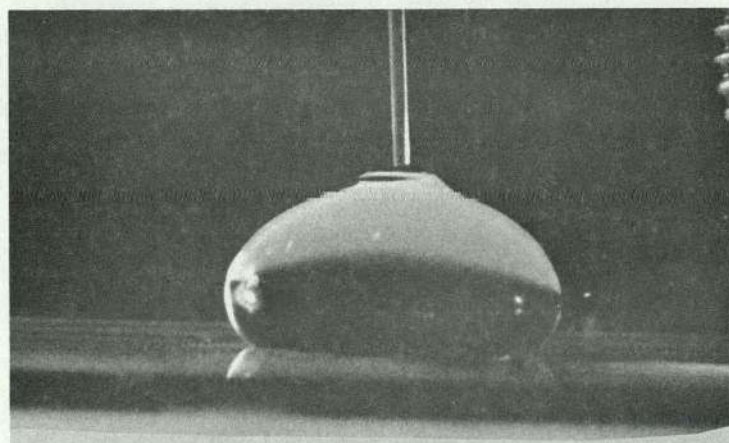
(8b)

Figure 11. Increased motion of positive-beta drop as solute touches
point of greater curvature.

as the radii of curvature at each point are determined.

The equations developed thus far deal with static drops and static forces. The dynamic drop at any time will be considered a static drop with dynamic pressures imposed on it. The behavior of the drop is much the same as a weight oscillating on a spring. At any time, the system may be described as a static system where a ficticious amount of weight is necessary to hold the spring in one of its dynamic positions.

For example, an equation describing the motion of such a system with no damping is

$$m \frac{d^2\xi}{dt^2} + k\xi = mg \tag{21}$$

If the first term, the dynamic term, is ignored, the magnitude of mg must vary so that it equals $k\xi$ at all times. For this system, the value of $k\xi$ will vary between zero and 2mg. Pursuing the analogy further, one finds that the effect of k and m is interchangable since any solution describing the motion of this system will depend only on the ratio, k/m.

The actual droplet system is described by the pressure obtained from figure 12a,

$$P_i = P_o + \sigma K \quad \text{or} \quad \Delta P = \sigma K. \tag{22}$$

If the interfacial tension is suddenly changed from σ to σ', the curvature K must change to K' in order for P to remain constant and

$$\Delta P = \sigma K = \sigma' K' \tag{23}$$

The shape of a drop with a changing interfacial tension is difficult to describe and the static equations are more adaptable to additional pressure terms. The dynamic pressure equivalent to an interfacial tension change must produce the same droplet shape at equilibrium. In other words, the pressure
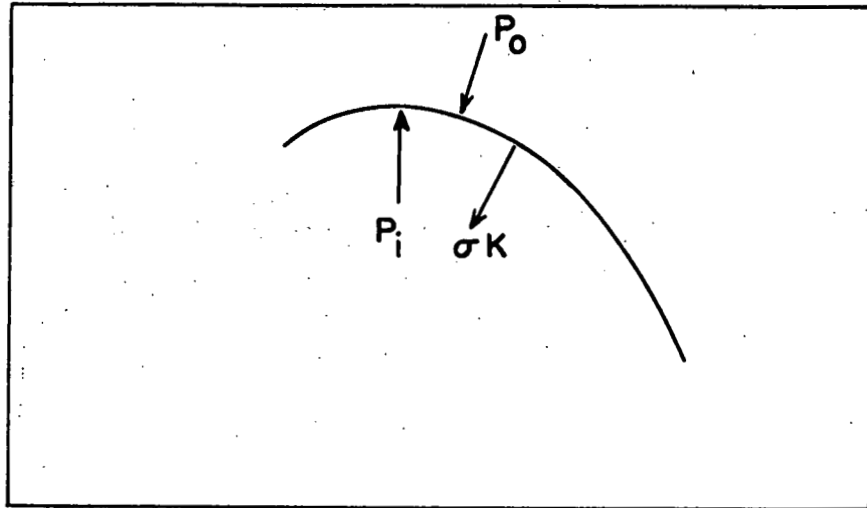
(12a)
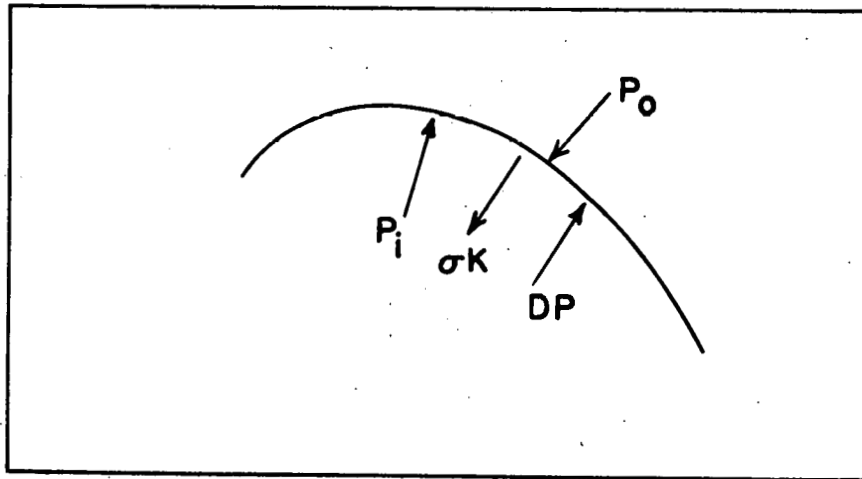
(12b)

Figure 12. Pressure balance on a static and a dynamic interface.

must change so the new equilibrium curvature, K', may be attained.

Thus, DP, the additional pressure, is the difference between the new and old static system pressures,

$$DP = \sigma K' - \sigma K \tag{24}$$

where σ does not change. Substituting equation (23) into equation (24) gives

$$DP = - \Delta\sigma K' = - \Delta\sigma \frac{\sigma}{\sigma'} K \tag{25}$$

and from a pressure balance in Figure 12b, the equation describing the dynamic drop in a quasi-static case is

$$P_i = P_o + \sigma K - DP.$$

The force actually varies as the height and curvature of the drop change, but the main concern is the pressure distribution necessary to hold the drop in a given shape if the drop were at equilibrium. The equilibrium equation to be solved is

$$P_o - P_i = \Delta P = \Delta P_o + \Delta\rho g z = \sigma K - \alpha DP,$$

where α represents the fraction of the initial force necessary to hold the drop a small distance from its initial position. At $z = 0$,

$$\Delta P_o = \frac{2\sigma}{b} - \alpha DP_o$$

and substituting for ΔP_o,

$$\frac{2\sigma}{b} + \alpha \, (DP - DP_o) + \Delta\rho gz = \sigma \, \left(\frac{1}{R_1} + \frac{1}{R_2} \right)$$

$$\frac{d\phi}{ds} = \frac{1}{R_1} = \frac{2}{b} + \frac{\alpha \, (DP - DP_o)}{\sigma} + \frac{\Delta\rho gz}{\sigma} - \frac{\sin \phi}{x} \qquad (26)$$

Now, α and b will be parameters subject to the boundary conditions,

1) known droplet volume,

2) known contact angle or measured base width, and

3) measured droplet height.

The solution was simplified by using the measured base diameter in place of known contact angle. The base width was found by actual measurements to remain constant during dynamic movement. Just as in the static drop with an external force, the actual pressure is not known but the distribution relative to the apex is known. The actual pressure and the shape are determined by the third boundary condition.

The development so far would be satisfactory for describing the shape of the drop if the movement were small and slow enough that inertia terms might be neglected. To extend the analysis to large deformations of the interface, the variation of driving force with solute movement and the effect of velocity components normal to the interface must be considered.

The solute spreads quite rapidly over the surface, causing both a variation in pressure drop and a change in area on which the pressure acts. Separate data were taken to measure the rate of solute spreading under the same conditions as those encountered by the drops, except the interface was flat. The interfacial velocity data were related to the interfacial tension gradient by considering the shear stress caused by a known

interfacial velocity. This approximate relation showed that the inter-facial tension distribution was non-linear. Appendix I provides many of the details of this analysis. The direction of the deviation from linearity was determined and a quadradic distribution was assumed. The spreading velocity data also made possible the calculation of the area influenced by the interfacial tension distribution as a function of time. Finally, an average pressure was calculated to account for the length of time a given area was under the influence of a given pressure change.

The normal velocity movement is also quite rapid. Because the initial movement of the apex of the drop is upward and outward, the constant volume restriction demands that there be a corresponding inward movement along the droplet surface. The position and distribution of the inward movement are unknown, but the form is that of a propagating wave. The solving of the wave equation including a variable impulse spreading over a changing area would be quite complex and has not been solved. Instead, the solution to a two dimensional wave equation as given by Lamb (9),

$$\delta = BJ_o(k's) \cos (\gamma t + \epsilon)$$

was used as a first approximation. At a given time and for a known amplitude, B_t, the displacement is

$$\delta = B_t J_o(k's). \tag{27}$$

The value of B_t is the distance the apex has moved over a specified time interval, Δt. The movement of the apex as a function of time was measured for several drops and these data are in Appendix II. The wave

displacement is important only in its relation to the pressure distribution along the interface. In this regard the assumption was made that the ratio of displacement to pressure change was constant along the interface. Since the pressure change and motion at the apex were known, the pressure at any point was given by

$$DP = \delta\left(\frac{DP_o}{B_t}\right) .$$

(28)

The dynamic pressure distribution is a function of time since its area of influence increases with time. The wave approximation is also a function of time since the wave is caused by the dynamic pressure. Over a very small time interval, the apex of the drop will move a distance, B_1. Over the same interval, the solute will have spread a distance, s_1; this increment has an assumed interfacial tension distribution, such that the droplet movement is outward over the whole increment. Thus the inward movement and inward pressure must begin for $s \geq s_1$, and $J_o(k_1's_1)$ must be zero at this point. Now, k_1' may be determined and B_t is known, so δ_1 may be calculated as a function of s by

$$\delta_1 = B_1 J_o(k_1's)$$

and the dynamic pressure distribution is

$$DP_1 = \delta_1 \times \frac{DP_o}{B_1} .$$

At the end of the succeeding time interval the interfacial tension change will cover a greater radius, s_2. However, an outward pressure does

not act over the whole distance since the previous distribution must be superimposed to get the final distribution. The distribution over each time interval is multiplied by the length of the time interval it acts, the distributions are summed, and then they are divided by the length of the total time interval. A value of s will exist where $\delta_2 = 0$, corresponding to $\Delta t_1 \times DP_1 + \Delta t_2 \times DP_2 = 0$ and k'_2 may be calculated. The dynamic pressure distribution used for the integration of a droplet profile is the one corresponding to the length of time the drop has been moving and is the combination of several superimposed distributions.

EXPERIMENTAL MEASUREMENTS

To compare the droplet shapes predicted by the model developed in the previous sections to actual droplet shapes, motion pictures were taken of drops moving under the influence of an interfacial tension change. As seen in the photographs in the section of dynamic drops, two liquid-liquid systems having inverse density and wetting characteristics were used.

The negative-beta system consisted of a cyclohexane drop and an aqueous continuous phase. The drop was held under water by a flat teflon plate which was preferentially wetted by the organic phase. The positive-beta system consisted of a carbon tetrachloride drop and an aqueous continuous phase. The drop rested on a glass plate which was preferentially wetted by the water. The solute used to change the interfacial tension was cyclohexanol for both drops. Each system was contained in a glass chamber, four inches on a side. The chamber was made from five optically flat pieces of glass glued together by Eccobond-26 epoxy resin. The resin had little effect on the interfacial tension. Earlier, a plexiglas chamber was used, but due to a surfactant material in the plexiglas, the interfacial tension of the liquids in the chamber was lowered as much as 10 dynes/cm.

Before each roll of film was taken, all parts of the system that contacted either liquid were thoroughly cleaned with chromic acid cleaning solution and rinsed with distilled water. All manipulations were carried out with as little time delay as possible to reduce any build-up of inter-facial contamination which would have greatly affected the interfacial tension and the interfacial response to surface active solutes.

The pictures were taken at 400 frames per second with a Milliken DBM5, pin registered motion picture camera. Lighting was accomplished by three General Electric photoflood lamps, one above and one on each side of the chamber, located approximately one foot from the chamber. The lights were used only during the actual filming; ten seconds are required to run one roll of film, so a negligible temperature change was brought about by heat from the lights. The lens opening was f/2.8 and the shutter speed was 1/2000th of a second.

A 1.0 microliter syringe was used to introduce solute at the droplet interface. Positioned exactly above the center of the drop, the syringe was fastened to a screw driven slide which was operated by a variable speed motor. Approximately one-half centimeter above the apex, a drop of solute was formed on the tip of the syringe. The drop was nearly spherical and was either 0.1 or 0.2 microliters in volume. The residence time of the drop in water was kept as small as possible since the cyclohexanol would transfer to the aqueous phase to some extent even though it was not appreciably soluble in the water. The syringe was lowered to the apex until the small drop coalesced with the large one (0.2 - 2.0 milliters). At the instant of coalesence droplet motion was initiated.

The motion picture negatives were projected frame by frame on white paper at a magnification of about twenty times actual size. Fine grain film was used to make the profiles of the drops as sharp as possible. These profiles were traced on the paper and measurements were taken from the tracing. The profiles of static drops measured before any motion had occurred were fit to the static equation by a two-parameter least squares

technique. The parameters were the interfacial tension and the radius of curvature at the origin. This was done to check the degree of interfacial contamination present. The volume was calculated by subdividing the drop into several elements approximated by frustra of right circular cones and summing their volumes.

In addition to droplet deformation, it was necessary to measure the rate at which the solute spread along the plane of the interface. Spreading data were taken in a round glass dish, three inches in diameter and one and one-half inches in height. The bottom of the dish was optically flat and the camera was positioned below the dish, perpendicular to the interface. Only one light was used and it was positioned above the interface so light would be reflected from the particles in the interface into the eye of the camera. Seventy-five milliliters of the heavier phase and fifty milliliters of the lighter liquid were poured into the dish. Eccospheres were placed on the interface and the camera was focused on the eccospheres. Eccospheres are tiny hollow glass spheres that give an overall appearance of a finely divided white powder. They come in a mixture of densities but a given density range may be separated by allowing them to settle in a liquid of known density. Since the volume of liquid was known, the dish could be cleaned and refilled after each run without refocusing the camera.

For each run, a small drop of solute was formed on the tip of the microliter syringe. With as little time lapse as possible the drop was moved to the interface until it coalesced and the subsequent motion of the eccospheres was recorded by the camera. The interfacial tension was measured before and after the solute was added to check for surface

contamination. All interfacial tension measurements were made with a DuNouy Ring Interface-Tensiometer.

The spreading data were measured by the same projection technique as used for dynamic drops. At each frame, the best circle was constructed through the ring of eccospheres that form the outer edge of spreading as shown in Figure 13. The radius of this circle will be referred to as the radius of spreading.
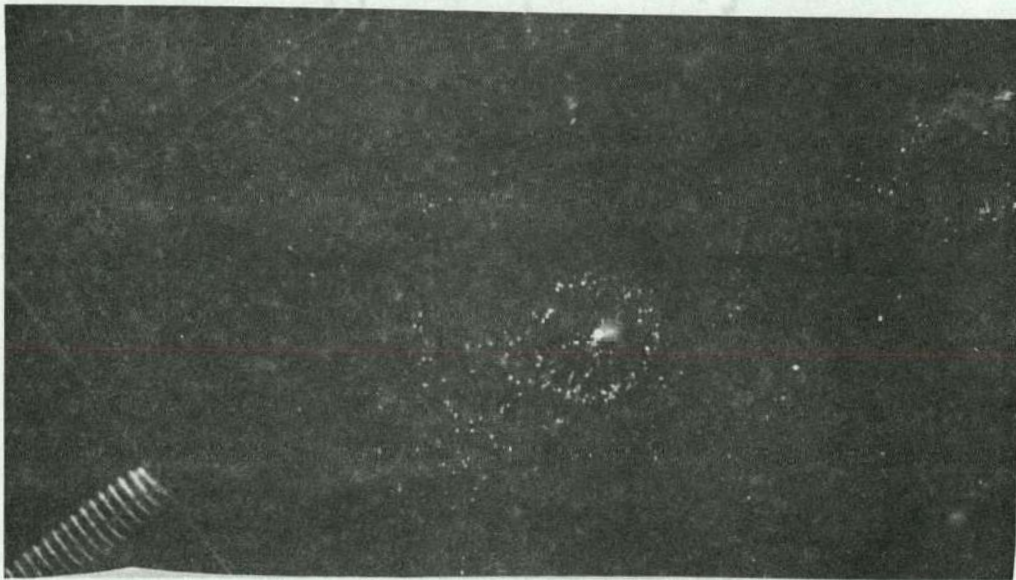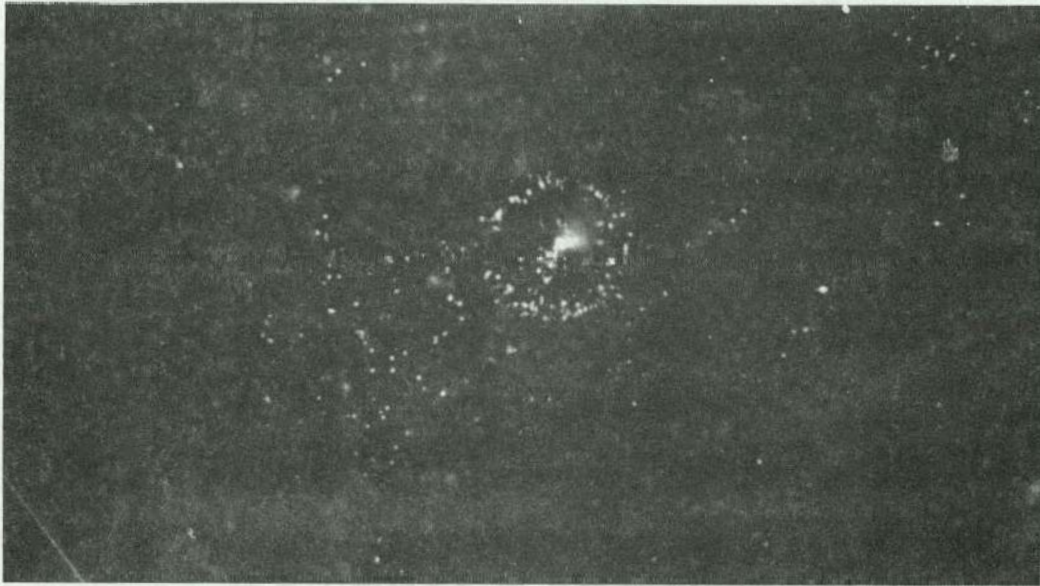
Figure 13. Movement of eccospheres in two consecutive frames at 400 frames/second.

RESULTS

The results in this section combine the analysis in the dynamic drops section with the data in the appendices to calculate the shapes of dynamic drops. The motions of a typical negative-beta drop (DD-15.2) and a typical positive-beta drop (DD-18.2) are followed and their behavior discussed over a 25 millisecond time interval.

Before the dynamic droplet profiles could be computed, the dynamic pressure distributions over the surface of the droplets had to be calculated by the procedure described in the dynamic drops section. This calculation required data on the movement of the apex as a function of time so that the wave amplitude, B_t, could be calculated. These data, presented in detail in Appendix II, are summarized for seven drops in Figure 14. The velocities at which the solute spreads on a flat interface were used to calculate the interfacial tension distribution. These measurements, found in Appendix I, were used along with the radii of curvature values calculated from the static droplet profile to calculate the change in pressure drop across the interface.

The droplet profiles were calculated at intervals of 5 milliseconds and each calculation required a different dynamic pressure distribution corresponding to a specific time. Four such pressure distributions are shown in Figure 15. The actual value of the dynamic pressure depends on the value of the coefficient α, which was arbitrarily set equal to 0.22 for this plot. The dynamic pressure, DP, for a short time interval (5 milliseconds) is compared to DP for a long time interval (25 milliseconds) for both drops. The shorter time intervals have the smaller radii of
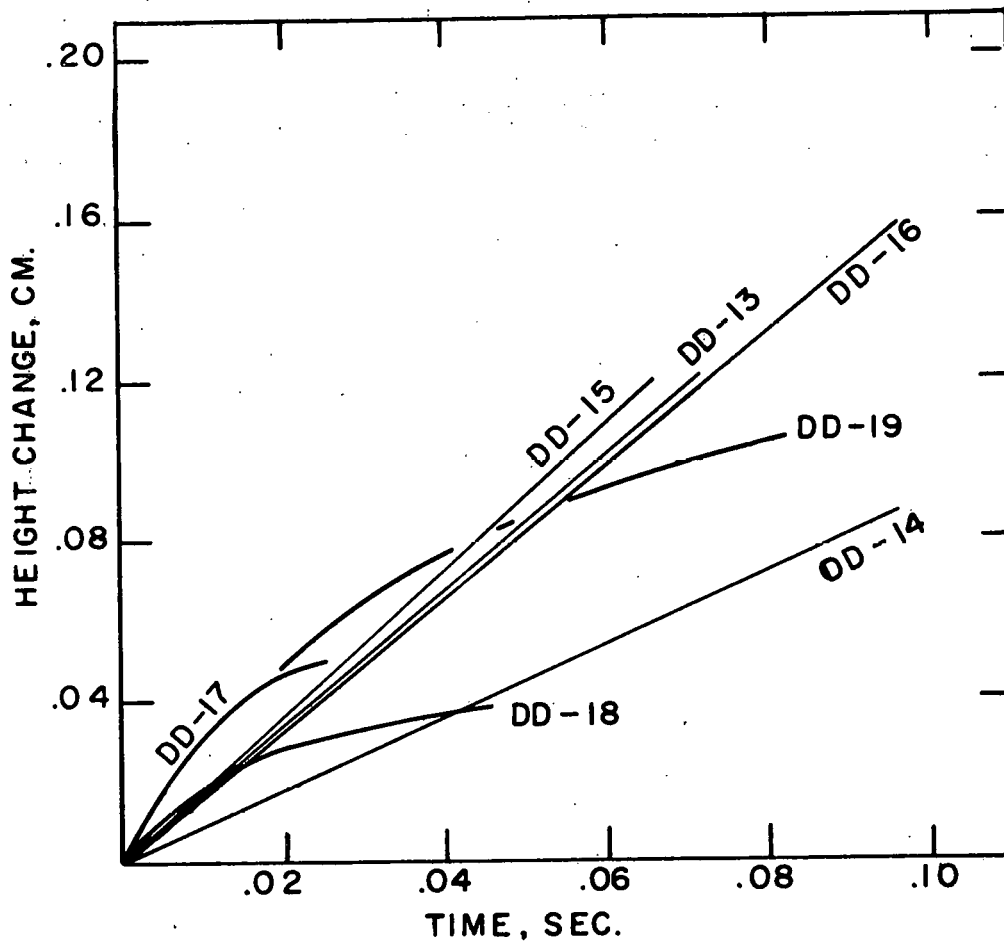
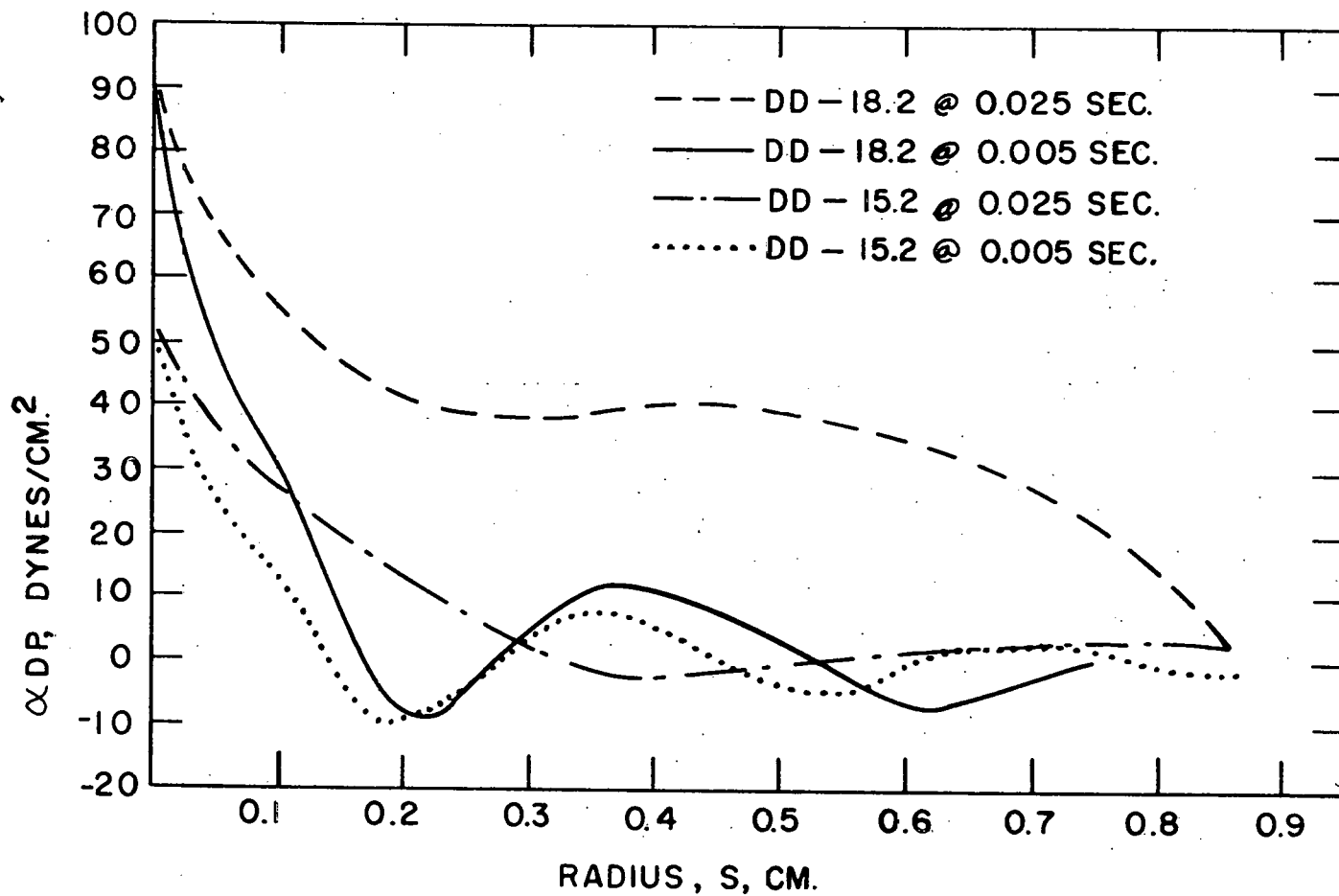Figure 14. The increase in the height of a dynamic drop versus elapsed time.

Figure 15. Dynamic pressure as a function of arc length for a positive-beta drop (DD-18.2) and a negative-beta drop (DD-15.2).

spreading, therefore the rate of change of DP with arc length is rapid since the total variation in interfacial tension covers a small distance. The total interfacial tension change--the difference between the new interfacial tension at the apex and the unchanged value at the outer edge of spreading--was assumed constant over the 25 millisecond time interval. At the later time, the total change in σ is unchanged, but it extends over a much larger distance. Thus, the slope of DP is not as steep as before.

The formation of a surface wave propagating from the apex of the droplet, causes DP to become negative at some value of s less than the radius of spreading. This tends to increase the slope of DP for all the curves and causes the value of DP to oscillate about the horizontal axis. Waves may actually be seen in motion pictures of the dynamic drops, but no attempt was made to compare these waves to the calculated pressure distribution. Later, the wave like portion of the dynamic pressure at large values of s will be shown to have little effect on the droplet shape, however.

In 25 milliseconds the solute had spread 0.8 centimeter over the negative-beta drop and 1.2 centimeters over the positive-beta drop. It should be noted that the arc length of the positive-beta drop is about 0.8 centimeter from apex to base, but the distribution was calculated on the basis that the extent of the interface was infinite. Again, the most significant fluctuations are those near the apex, so small errors in DP near the base should have little effect on the shape of either drop.

The total change in the value of the interfacial tension was assumed to be constant throughout the whole time interval. Evidence verifying the

assumption comes from two sources. As shown in Appendix II the spreading rate is nearly independent of the volume of solute; the spreading rate depends only on the solute concentration for the experiments performed. The graphs in Appendix I show the rate of apex movement to be nearly independent of the volume of solute. The 0.2 microliters of solute must surely be able to hold the concentration constant for a longer time than the 0.1 microliters of solute, but both produce the same response. This tends to justify the assumption that the concentration remained constant at its initial value at the apex over the 25 millisecond time interval.

Since the interfacial tension change is approximately the same for both drops, the magnitude of DP at the origin differs for the two drops due to differences in curvature. The positive-beta drop, having the greater curvature, also tends to have a more rapid decrease in DP with arc length. However, the higher rate of spreading found in the positive-beta system tends to counteract the effect of different curvatures when the two drops are compared at the same time.

The distributions were calculated at 5, 10, 15, 20, and 25 milliseconds for each drop. These intervals along with the corresponding droplet heights are given in Table I. Then the droplet profiles were calculated at each time interval. The procedure involved a nested iteration to solve for the parameters b and α. A value of α was assumed; then b was adjusted to satisfy the droplet height and base diameter boundary conditions. The resulting volume of revolution was calculated and plotted against α as shown in Figures 16 and 17. The intersection of this plotted curve with the line representing the actual droplet volume determined the value of α.
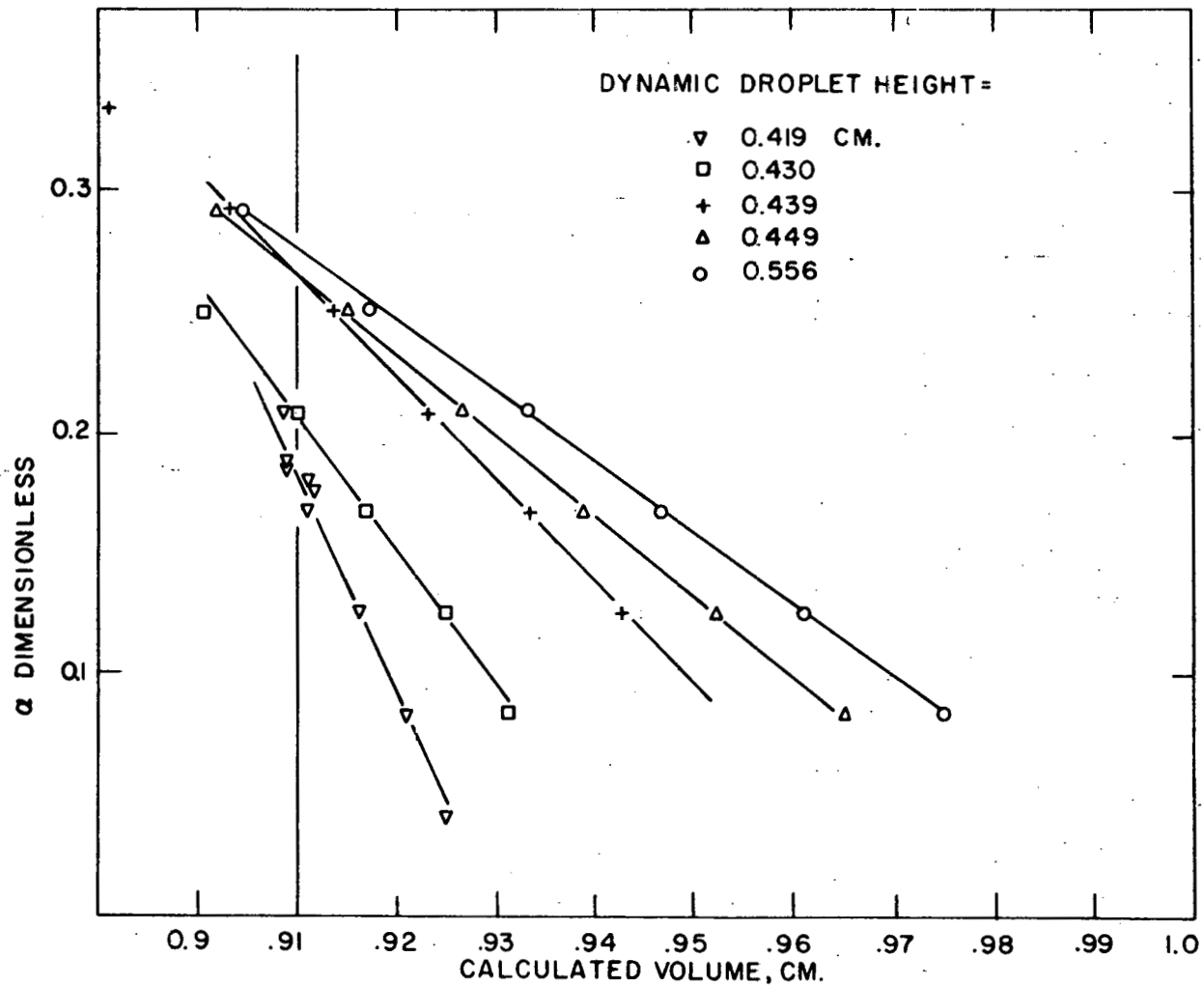
Figure 16. Determination of α for the negative-beta drop (DD-15.2) at equal
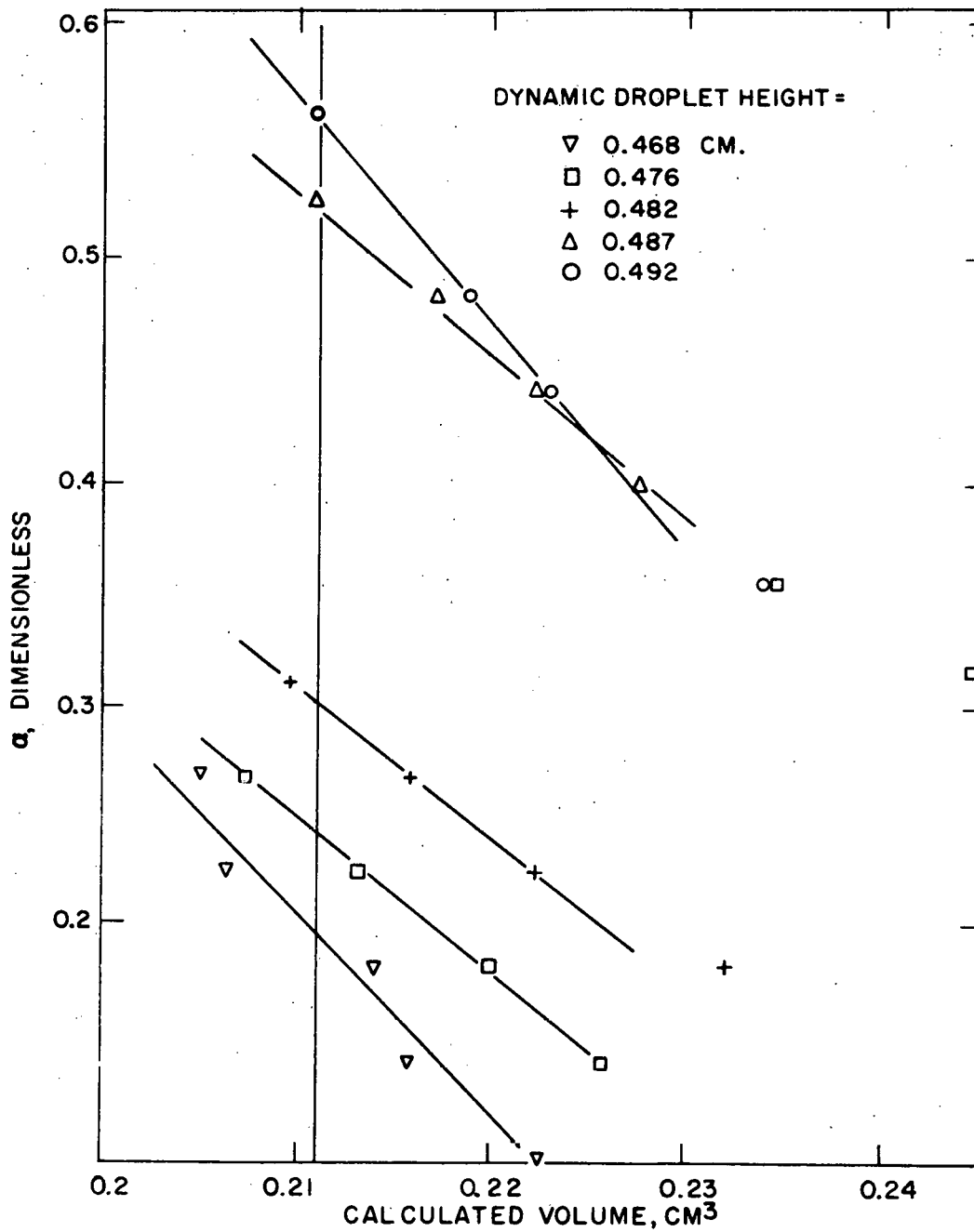time intervals of 5 milliseconds.

Figure 17. Determination of α for the positive-beta drop (DD-18.2) at equal time intervals of 5 milliseconds.

The lack of smoothness of the plotted points is due to the large tolerance used when satisfying the boundary conditions in keeping with the integration step size. The values of α and b are also given in Table 1.

Alpha increases from zero as the drop leaves its static shape. Actually, α has no meaning for the original static drop, but if dynamic pressures were present, α would be zero and the external force required to hold the drop in its present position would be zero. At a later time, the magnitude of the force to hold the drop in its present position would be given by

$$F = \int_S \alpha \, DPdS$$

Table 1. Dynamic droplet parameters

Drop No.	Elapsed time, seconds	Droplet height, cm.	b, cm.	alpha
DD-15.2	0.0	0.414	1.28	--
Cyclohexane - water	0.005	0.419	.76	0.184
	0.010	0.430	..70	0.209
	0.015	0.439	.62	0.265
	0.020	0.449	.59	0.265
	0.025	0.456	0.60	0.276
DD-18.2	0.0	0.458	.66	--
Carbon tetrachloride- water	0.005	0.4675	.43	0.196
	0.010	0.4755	.42	0.243
	0.015	0.482	.38	0.303
	0.020	0.4865	.36	0.531
	0.025	0.492	.32	0.575

To understand the effect of the dynamic pressure distribution on the shape of the calculated profile, the differential equation which describes the profile can be examined:

$$\frac{d\Phi}{ds} = \frac{2}{b} - \frac{\sin \Phi}{x} + \frac{\Delta\rho g z}{\sigma} + \frac{\alpha(DP - DP_o)}{\sigma} \tag{29}$$

The rate of change of the slope of the plotted droplet profile is a measure of $d\Phi/ds$, the curvature of the profile. Consider first the negative-beta drop (DD-15.2). Figure 18 shows the measured dynamic drop compared to the static drop and the calculated dynamic drop. The radius of curvature at the apex decreases as the drop increases in height. In order for the boundary conditions at the base to be met, $d\Phi/ds$ must decrease at a faster rate than would a static drop.

The second term on the right dominates in the beginning of the calculation when $z = 0$ and $DP = DP_o$, but as the calculation proceeds the third term quickly dominates. Both terms are negative, however, and tend to decrease the curvature. Now the fourth term determines how the drop will deviate from a static drop and its magnitude must be large enough to be non-negligible compared to the other terms.

The fourth term in equation (29) has the same effect in the positive-beta drop as it does in the negative-beta drop except it must oppose the third term which is positive and twice as large in magnitude for the systems used in this work. Figure 18 compares the calculated profile at 25 milliseconds to the measured profile at the same time. The deviation of the calculated and measured profiles in Figures 18 and 19 will be
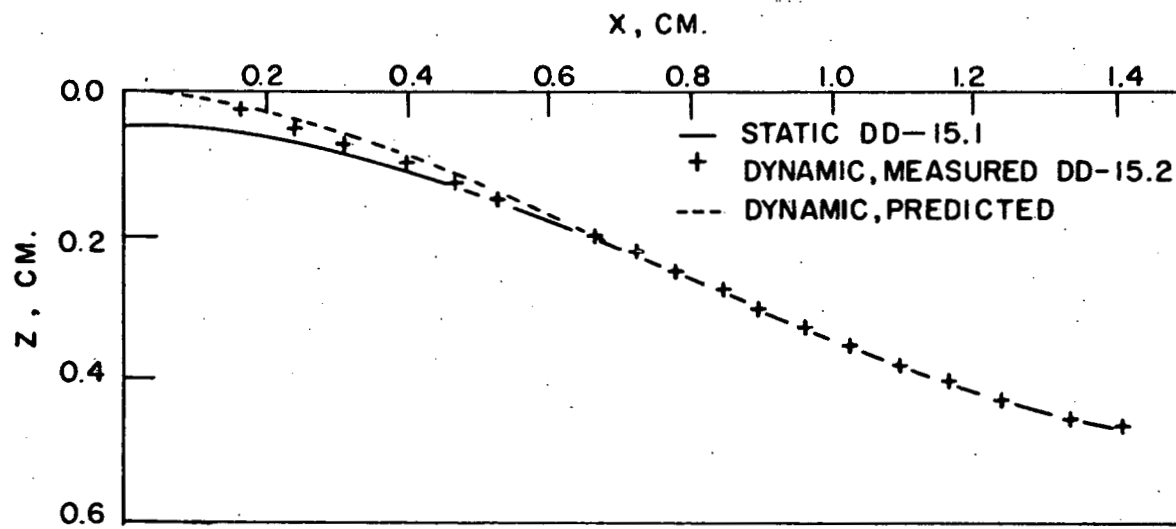
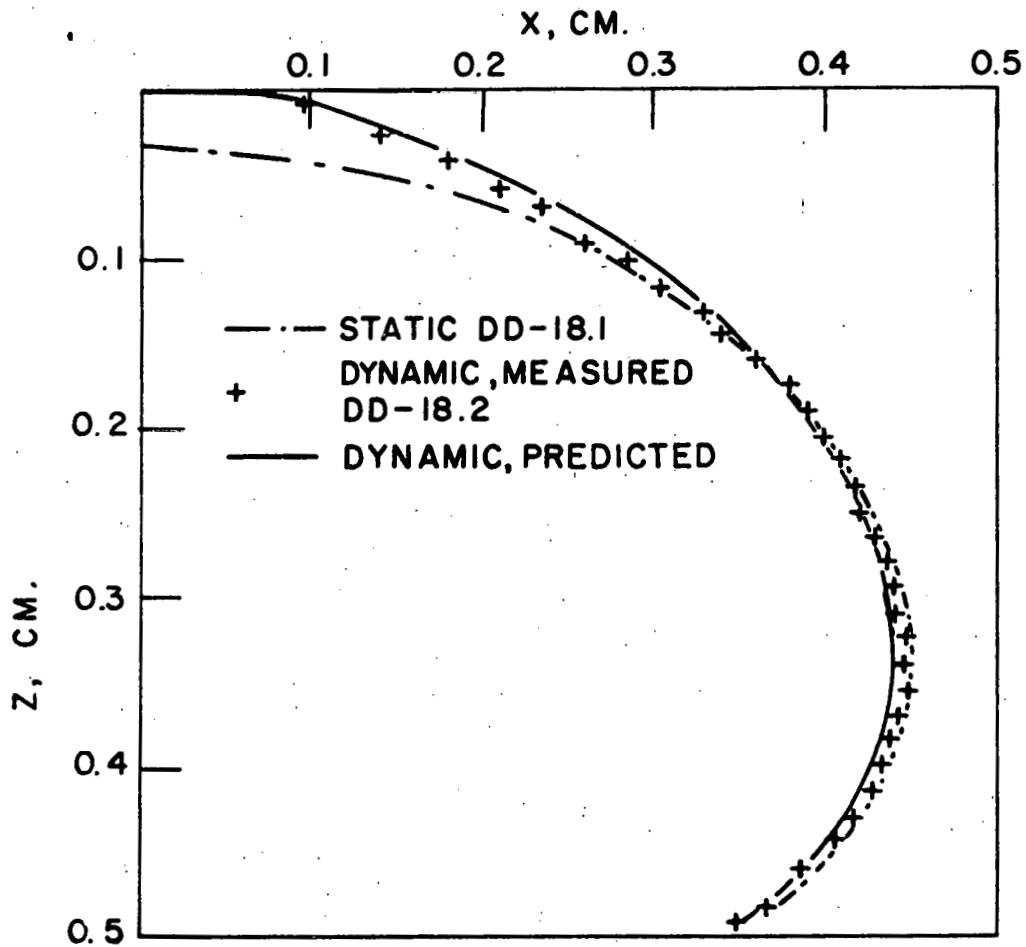Figure 18. The negative-beta dynamic drop after 25 milliseconds.

Figure 19.   Positive-beta dynamic drop after 25 milliseconds.

discussed in reference to the effect of DP and α.

Figure 15 shows that the value of DP at s = 0 (DP_o) is the greatest value of DP; therefore the fourth term begins at zero and is negative at all other values of s. At the base of the positive-beta drop, the numerator of the second term in Equation (29) has a value of about 400 dynes/cm.^{2}, and fluctuations in the numerator of the fourth term decrease quite rapidly such that it has negligible effect on the droplet shape near the base of the drop (s = 0.8 cm.) even though the magnitude of the fourth term is large.

The rate of change of the fourth term is not large enough in either drop since the slope of the calculated profile does not decrease rapidly enough to allow a smaller value of b. An increase in α would satisfy this change in shape by the increase in αDP, but the boundary conditions would not be satisfied. The only alternative would be to change the pressure distribution to have a more rapid initial slope such as it had, for example, at 5 milliseconds. This shows, then, the error in the pressure distribution and how it should be changed or what changes a better model would provide.

The importance of having the proper pressure distribution was established by trying a linear distribution and finding that no values of b and α would satisfy the boundary conditions for the negative-beta drop. Similarly, for the positive-beta drop the comparison to the data in Figure 20 was not as good as the comparison in Figure 19 where the dynamic pressure distribution was predicted by the model.

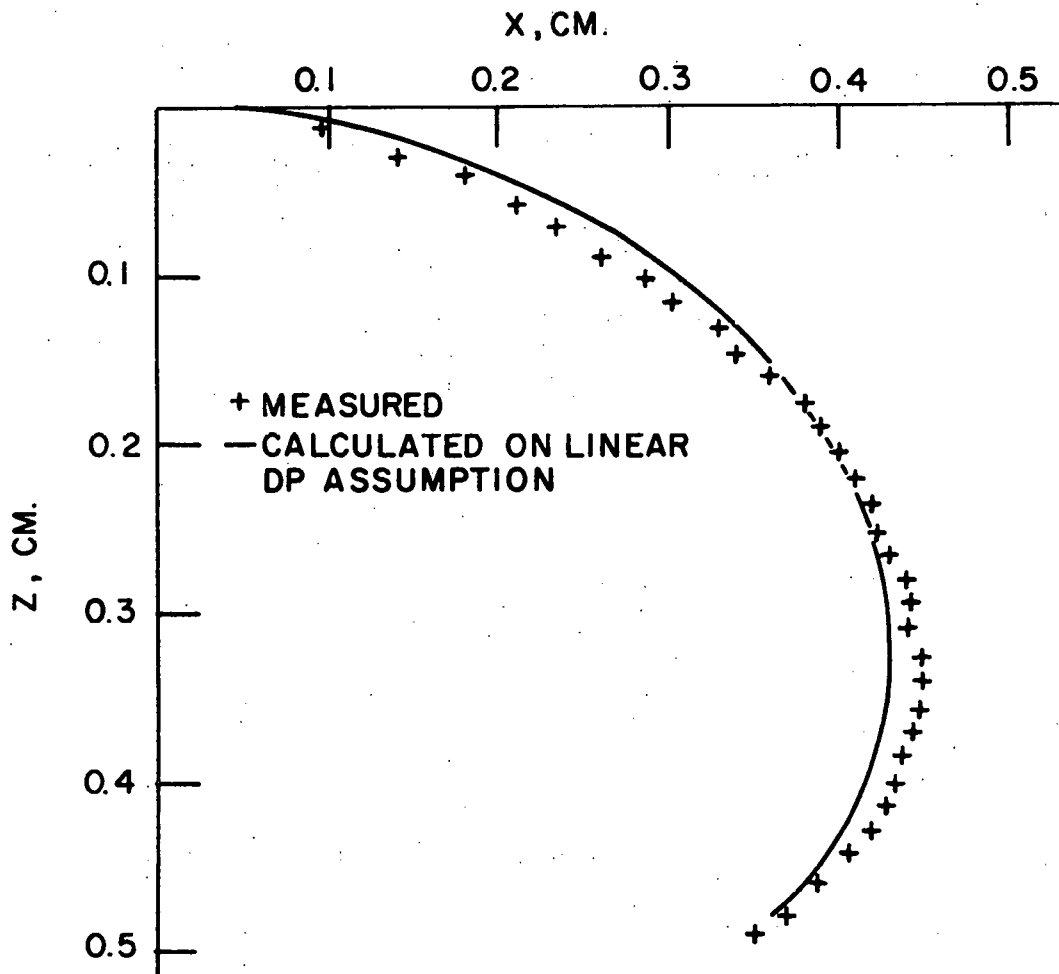Both the relative distribution of DP and the value of α influence the

Figure 20. Positive-beta dynamic drop after 25 milliseconds compared to a drop with a hypothetical dynamic pressure distribution.

rate at which the curvature decreases relative to the static drop. From
the spring analogy one reasons that α should increase as droplet height
increases and that its maximum value would be 2.0 if the system were un-
damped. As time increased, the pressure distribution tended to change less
rapidly with arc length, but the description of a dynamic drop required the
opposite trend in αDP. Therefore, α was forced to increase so the fourth
term would have increasing effect as the droplet height increased. Alpha
may have increased faster in the beginning of movement since, unlike the
spring, there are two ways for dynamic pressure to be absorbed into the
system, by an increase in curvature and by an increase in hydrostatic
pressure.

In both drops, α increased while b decreased, but the value of b
became almost invariant and may even have shown a tendency to increase for
the negative-beta drop at 25 milliseconds. Some of the dynamic pressure
absorbed by an increase in curvature may have been converted to hydrostatic
pressure and as α increased, b also increased. The curvature at the apex
of a separating drop also goes through a minimum.

Turning again to Figure 14, the velocity at the apex of all the
positive-beta drops tends to decrease quite rapidly compared to the
velocities of the four negative-beta drops represented by straight lines.
This difference in behavior must be due to the different density character-
istics, since the pressure change at the apex is less for the negative-beta
drops than for the positive-beta drops. The decrease in interfacial tension
makes an increase in height the easiest reaction for the negative-beta drop
whereas a great deal of force is required to lift the heavy organic of the

positive-beta drop. Figures 18 and 19 indicate that the model holds equally well in both systems, however,

The density difference is also reflected in the static curvatures. The curvature of a positive-beta drop increases as a function of s, whereas the curvature of a negative-beta drop decreases as a function of s and will even become negative before the base of the drop is reached. The pressure change associated with a given interfacial tension change depends on the value of the curvature. So, after solute has spread to the side of the positive-beta drop where the curvature is larger than at the apex, the pressure change is greater and the horizontal force becomes greater than the vertical force and the drop will stop rising and begin to flatten. The negative-beta drop behaves in an opposite manner in that the negative curvature near the base will produce a negative velocity when an interfacial tension change occurs. Thus the original upward movement of the apex is reinforced.

In comparing the movement of the positive-beta drop to the negative-beta drop, Table 1 shows that the value of α at 25 milliseconds is greater in the positive-beta system. The positive-beta drop has attained a large fraction of its maximum height in 25 milliseconds as shown in Figure 14 on curve DD-18.2. In constrast, over the same time interval, the negative-beta drop shown by curve DD-15.2 has not approached its maximum value of 0.6 centimeters. Because of viscous damping, α remained considerably less than 2.0 for both drops.

The model applies equally well for both droplet systems, but the calculated profiles deviate slightly from the measured droplet profiles.

These deviations come primarily from the approximations used for three significant effects:

1) the use of a surface wave to approximate dynamic pressures

2) the assumed interfacial tension distribution

3) exclusion of viscosity effects.

The dynamic pressure was substituted for the decrease in the ability of a perturbed interface to hold its static shape. The additional dynamic pressure arising from the propagating wave was opposed by the original interfacial tension. This part of the dynamic pressure should have been opposed by smaller interfacial forces since the interfacial tension had significantly decreased in the neighborhood of the apex.

The wave used in the model was a simple oscillatory wave, but a propagating wave produced by a varying impulse would have been used if a solution were available. A propagating wave would have a steeper slope at the origin and a smaller, but longer negative deviation from the original surface. However, both waves adhere to the restriction of constant volume. The propagating wave would give a more rapid variation of DP with s near the apex.

A more rapid variation in interfacial tension would also improve the dynamic pressure distribution. The analysis in Appendix II shows that the distribution of interfacial tension is at least quadradic, but it may even be greater.

The effects of viscosity have not been explicitly included in this investigation. However, viscosity would be expected to greatly affect the rate of droplet movement, especially at the apex where the velocity is

greatest. The movement of the apex was measured and used as a boundary condition, thus avoiding the major viscous effects. However, the effects of viscosity on the dynamic pressure distribution or on the propagating wave were not considered.

CONCLUSIONS

Because of the complexity of the problem, a complete description of
a dynamic drop will require much additional work, but some of the basic
mechanisms involved have been outlined and studied in this work.

A non-uniform interfacial tension imposed on a drop will cause it to
seek a new equilibrium shape. At any time during the initial motion, the
drop may be considered a static drop with a dynamic pressure distribution
imposed on it. This is made possible by adding the boundary condition of
droplet height and solving for α, the fraction of the initial pressure
impulse needed to hold the drop at the known height. The two most signifi-
cant factors taken into account in calculating a dynamic pressure distri-
bution are:

1) the change of interfacial tension with time and arc length

2) the formation of a wave propagating from the apex.

The calculated values of α and the favorable comparison of calculated
droplet profiles to actual drops show that these two factors are signifi-
cant. The model could be improved in both areas, and the improvements
were shown to be such that the description of the droplet profile would be
improved.

The model approaches its limit of applicability at 25 milliseconds
since α is becoming too large and additional mechanisms will begin to
appear. The interfacial tension change at the origin will decay and the
entire distribution of interfacial tension will change. The direction of
apex movement will change and the droplet will begin to oscillate.

Experimentally, it was found that an increase in solute concentration for the systems used increased the distance and time of spreading significantly, whereas an increased volume of solute had only a small effect. The movement of the apex under dynamic conditions for a negative-beta drop was nearly linear with time. The positive-beta drop showed definite deceleration at the apex. The difference was due to the greater effect of hydrostatic pressure effect in the positive-beta system. The volume of solute, again as in spreading, had little effect on droplet motion while the change in solute concentration had a significant effect.

RECOMMENDATIONS

An attempt has been made in this work to simplify the analysis of the problem as much as possible and only pressures considered significant have been included. If the correct dynamic pressure distribution and height were known exactly, then the previous analysis would enable the calculation of the actual shape of the dynamic drop. Toward this end, the two major phenomena of solute spreading and apex movement should be isolated and studied in detail.

1) A two dimensional model could be developed to describe the motion of solute spreading on a flat interface between two liquids. The model should relate the interfacial velocity to the interfacial tension at any point along the radius of spreading. Then one might study an interface that has solute transferring across it. A measurement of interfacial velocity fluctuations could be related to interfacial tension and concentration fluctuations that might occur in large scale mass transfer equipment.

2) The movement of the apex should be predicted from the knowledge of the interfacial tension change and the curvature. The predictions should also be based on the physical properties such as the densities and viscosities of the two phases. The initial approach should be an impirical correlation of apex velocities for several systems having a wide variation in physical properties. Then perhaps a mathematical model could be developed that would consider the effect of the interfacial resistance to motion caused by a change in interfacial tension.

A description of the wave propagating from the apex could be found by solving the wave equation with the condition of a prescribed impulse that varies in magnitude along various portions of the drop. The resulting pressure change could be calculated from equations describing the wave.

NOMENCLATURE

A	vertical area component, $cm.^2$
A_h	cross sectional area of drop at $z = h$, $cm.^2$
A_o	cross sectional area at $z = 0$, $cm.^2$
b	radius of curvature at origin, cm.
B	wave amplitude, cm.
B_t	wave amplitude at origin at a given time, cm.
DP	dynamic pressure, $dynes/cm.^2$
F	net vertical force on drop, dynes.
$\vec{F}$	force vector, dynes
F_b	bouyant force, dynes
F_e	external force imposed on drop, dynes
F_T	total force on a portion of a drop, dynes
g	gravitational constant, $cm./sec.^2$
h	vertical distance from apex to an arbitrary point on drop, cm.
k	spring constant, $gm./sec.^2$
K	total curvature, 1/cm.
k'	wave number, 1/cm.
$\vec{n}$	unit normal vector to surface, S.
P_{o_o}	pressure at origin (outside drop), $dynes/cm.^2$
P_{o_i}	pressure at origin (inside drop), $dynes/cm.^2$
P_i, P_i'	inside droplet pressure, $dynes/cm.^2$
P_o	outside droplet pressure, $dynes/cm.^2$
r	radius of curvature of sphere, cm.
R_1	radius of curvature in plane of paper, cm.

R_2	radius of curvature revolves around center line, cm.
R_A	radius of curvature of drop in partition A, cm.
R_B	radius of curvature of drop in partition B, cm.
R_{10}, R_{20}	radius of curvature at $z = 0$, cm.
s	arc length, cm.
S	surface area, cm.^{2}
t	time, sec.
V_s	spreading velocity, cm./sec.
W	weight, dynes
x	horizontal coordinate, cm.
x_h	horizontal coordinate at $z = h$, cm.
x_o	horizontal coordinate at $z = 0$, cm.
z	vertical coordinate, cm.
α	dimensionless coefficient, fraction of total force used from that available from initial impulse on static drop.
γ	frequency, 1/sec.
ΔP	pressure drop across interface, dynes/cm.^{2}
$\overline{\Delta P}$	average pressure drop across element of interface, dynes/cm.^{2}
$\Delta \sigma$	change in interfacial tension, dynes/cm.
ϵ	phase angle, radians
μ	viscosity, poise
ξ	vertical displacement, cm.
ρ_d	density of drop, gm./cm.^{3}
ρ_c	density of continuous phase, gm./cm.^{3}
σ, σ'	interfacial tension, dynes/cm.

σ_A interfacial tension between two liquids in partition A, dynes/cm.

σ_B interfacial tension between two liquids in partition B, dynes/cm.

Φ angular coordinate, radians

Φ_h angular coordinate at $z = h$, radians

Φ_o angular coordinate at $z = 0$, radians

δ wave displacement, cm.

negative-beta   carbon tetrachloride drop in water

positive-beta   cyclohexane drop in water

LITERATURE CITED

1. Bashforth, F. and Adams, J. An attempt to test the theories of capillary action. Cambridge, England, University Press. 1883.

2. Block, M. J. Surface tension as the cause of Bénard cells and surface deformation in a liquid film. Nature 178: 650-651. 1956.

3. Ellis, S. R. M. and Biddulph, M. Interfacial turbulence measurements. Chemical Engineering Science 21: 1107-1109. 1966.

4. Eskinazi, S. Vector mechanics of fluids and magnetofluids. New York, N.Y., Academic Press Inc. 1967.

5. Garner, F. H., Nutt, C. W., and Mohradi, M. F. Pulsation and mass transfer of pendant liquid drops. Nature 175: 603-604. 1955.

6. Goldstein, S. Modern developments in fluid dynamics. Vol. 1. New York, N.Y., Dover Publications, Inc. 1965.

7. Haydon, D. A. Oscillating droplets and spontaneous emulsification. Nature 176: 839-840. 1955.

8. Haydon, D. A. and Davies, T. V. An investigation of droplet oscillation during mass transfer. Royal Society Proceedings, Series A, 243: 483-499. 1957.

9. Lamb, Sir Horace. Hydrodynamics. 6th ed. New York, N.Y., Dover Publications, Inc. 1932.

10. Landau, L. D. and Lifshitz, E. M. Course of theoretical physics. Vol. 6. Fluid mechanics. Reading, Mass., Addison-Wesley Publishing Company, Inc. 1959.

11. Lewis, J. B. The mechanism of mass transfer of solutes across liquid-liquid interfaces. Chemical Engineering Science 3: 248-278. 1954.

12. Lewis, J. B. and Pratt, H. R. C. Oscillating droplets. Nature 171: 1155-1156. 1953.

13. Orell, A. and Westwater, J. W. Spontaneous interfacial cellular convection accompanying mass transfer: Ethylene glycol-acetic acid-ethyl acetate. American Institute of Chemical Engineers Journal 8: 350-356. 1962.

14. Pearson, J. R. A. On convection cells induced by surface tension. Journal of Fluid Mechanics 4: 489-500. 1958.

15. Pétré, G. and Schayer-Polischuk, M. L. Évolution controlée d'une goutte touchée localement par un tensioactif. Journal de Chimie Physique et de Physiocochimie Biologique 63: 1409-1415. 1966.

16. Rayleigh, Lord. On convection currents in a horizontal layer of fluid when the higher temperature is on the under side. The Philosophical Magazine and Journal of Science, Series 6, 32: 529-546. 1916.

17. Sawistowski, H. and Glotz, G. E. The effect of interface phenomena on mass transfer rates in liquid-liquid extraction. Institution of Chemical Engineers Transactions 41: 174-181. 1963.

18. Scriven, L. E. Dynamics of a fluid interface. Chemical Engineering Science 12: 98-108. 1960.

19. Scriven, L. E. and Sternling, C. V. The Marangoni effects. Nature 187: 186-188. 1960.

20. Sherwood, T. K. and Wei, J. C. Interfacial phenomena in liquid extraction. Industrial and Engineering Chemistry 49: 1030-1035. 1957.

21. Sternling, C. V. and Scriven, L. E. Interfacial turbulence: hydrodynamic instability and the Marangoni effect. American Institute of Chemical Engineers Journal 5: 514-523. 1959.

22. Suciu, D. G., Smigelschi, O., and Ruckenstein, E. On the structure of dissolving thin films. American Institute of Chemical Engineers Journal 15: 686-689. 1969.

23. Suciu, D. G., Smigelschi, O., and Ruckenstein, E. Some experiments on the Marangoni effect. American Institute of Chemical Engineers Journal 13: 1120-1124. 1967.

24. Thomson, J. On certain curious motions observable at the surfaces of wine and other alcoholic liquors. Philosophical Magazine, Series 4, 10: 330-333. 1855.

25. Valentine, R. S., Sather, N. F., and Heidiger, W. J. The motion of drops in viscous media. Chemical Engineering Science 20: 719-728. 1965.

26. Zuiderweg, F. J. and Harmens, A. The influence of surface phenomena on the performance of distillation columns. Chemical Engineering Science 9: 89-103. 1958.

ACKNOWLEDGMENTS

APPENDIX I

Solute spreading data reported here were used to determine the interfacial tension distribution over the surface of a liquid drop. All the data were taken on a flat interface, since the camera could focus only on a single plane. The data on the flat interface was then assumed to be valid on a curved interface, since the curvature was small compared to the thickness of the interface. Eccospheres--hollow glass spheres of small diameter--which had densities between the densities of the two liquids were assumed to move at the interfacial velocity even though they were preferentially wetted by water. The only measurement that could be obtained from the movement of these particles was position at various times; this enabled the calculation of interfacial velocity which in turn was assumed to be related to the interfacial tension.

The tendency for a solute to spread is determined by the free energy change associated with the spreading. For example, consider a lens of benzene floating on a water surface. Whether the benzene will spread or not depends on the free energy change associated with the formation of an air-benzene and a water-benzene interface and the free energy change associated with the elimination of an air-water interface.

$$dG = \left(\frac{\partial G}{\partial A_{AW}} \right) dA_{AW} + \left(\frac{\partial G}{\partial A_{BW}} \right) dA_{BW} + \left(\frac{\partial G}{\partial A_{AB}} \right) dA_{AB}$$

where

G is free energy

A_{AW} is area of air-water interface

A_{BW} is area of benzene-water interface

A_{AB} is area of air-benzene interface

$dA_{BW} = -dA_{AW} = dA_{AB}$

By definition,

$$- \left(\frac{\partial G}{\partial A_{BW}} \right) = S_{B/W}$$

where $S_{B/W}$ is the spreading coefficient of benzene on water. If $S_{B/W}$ is positive, the spreading will occur spontaneously.

$$S_{B/W} = \sigma_{WA} - \sigma_{BA} - \sigma_{BW}$$

where interfacial tensions are substituted for free energy per unit area.

From the development by Scriven (18), one finds that the rate of spreading depends on the surface tension gradient and the viscous resistance of the fluids adjacent to the interface. The drag force is equal to the surface tension gradient times the area.

With the aid of some simplifying assumptions, the drag force may be related to the interfacial velocity. The assumptions are:

1) The surface of the drop may be approximated by a flat surface.

2) The interface is made up of several circular flat plates as shown in Figure 21. These move a short distance in the radial direction without change in surface area.

3) The development by Blasius in (6) for the drag on a constant velocity, flat plate immersed in a liquid may be applied. He gives the drag on one side of a flat plate to be

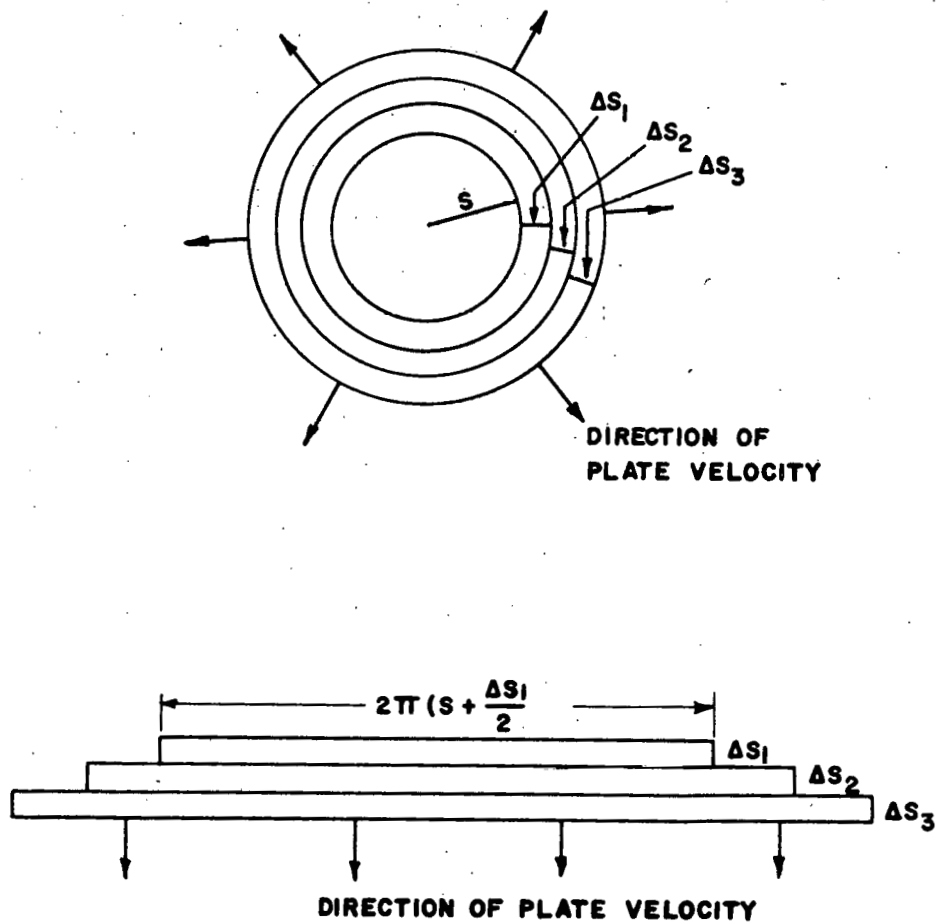$$F_D = 2\pi s \, (0.664) \sqrt{V_s^3 \mu \rho \Delta s}$$

Figure 21. Model used to calculate drag force from interfacial velocities.

where

F_d is drag force

s   is distance from center of spreading

V_s is surface velocity in the s direction

μ is viscosity

ρ is density

The surface stress can be expressed as $\tau = \dfrac{\Delta\sigma}{\Delta s} = F_D/2\pi s\Delta s.$

Therefore,

$$\frac{\Delta\sigma}{\Delta s} = 0.664 \sqrt{V_s^3 \, \frac{\mu\rho}{\Delta s}} \quad .$$

For a given system and equal increments of Δs, then:

$$\frac{\Delta\sigma}{\Delta s} \approx V_s^{3/2} \quad .$$

Only the interfacial tension at the origin and at the edge of spread-
ing is known. At the origin, the interfacial tension is determined by the
concentration of solute imposed there. Since the value of σ varies little
at high concentrations it was assumed constant for the initial movements.
(The values of σ versus concentration shown in Figure 22 are equilibrium
values measured with the ring tensiometer.) At the edge of spreading the
velocity is zero, then $d\sigma/ds = 0$ and the interfacial tension is the same as
the initial static value. The next problem, then, is to find the values
of σ between the two end points.

When solute spread, it cleared all the eccospheres from the area of
the origin, thus forming a radius of spreading as shown in Figure 13.
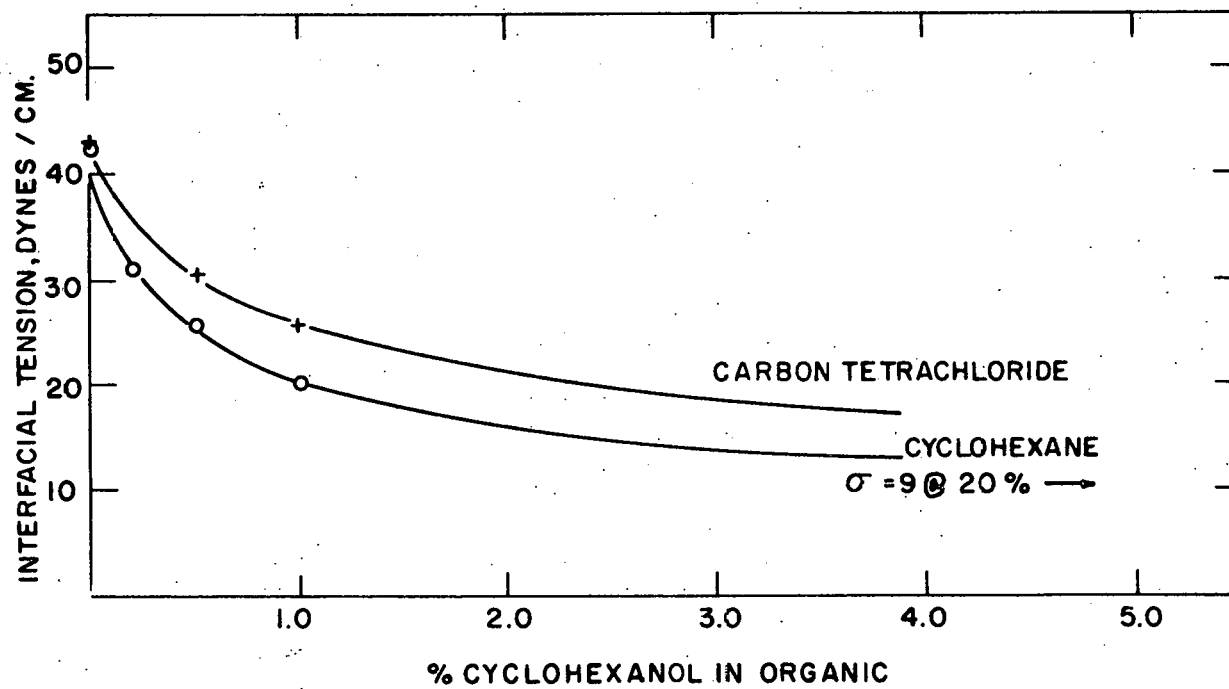
Figure 22. Equilibrium interfacial tension versus cyclohexanol concentration
for the positive-beta system and the negative-beta system.

Since there were no particles within this radius, no velocity measurements could be made for the time interval and position where no particles are present. The small quantity of solute (0.2 microliters) and small diameter needle made it impossible to inject particles along with the solute. However in separate experiments, particles were added to a propionic acid solute injected by a glass tube with a diameter of approximately 0.1 centimeters to a carbon tetrachloride-water interface. Figure 23 shows typical results. The initial increase in V_s indicates an acceleration from the origin where $V_s = 0$. If V_s were constant over a large range of s, $d\sigma/ds$ could be assumed constant, i.e., σ would vary linearly with s. This is not the case and since V_s versus s showed a non-linear decrease in V_s, one may conclude that the variation of σ with s is less than $s^{2/3}$ or perhaps $s^{1/2}$. This may be a good approximation since in spreading, the area covered by the solute increases as s^2. Actually, the variation may be greater due to the non-linearity of σ as a function of concentration. The dissolution of solute into the bulk liquid where the rate of dissolution will depend on the concentration would also be a factor. The quadradic distribution will give a good approximation since the end points are known and the direction of the deviation from linearity is known.

To coincide with the conditions on the dynamic drops, the experimental conditions outlined in Table 2 were imposed on a flat interface. The data taken from the conditions of Table 2 are shown as the radius of spreading versus time in Figures 24 and 25.
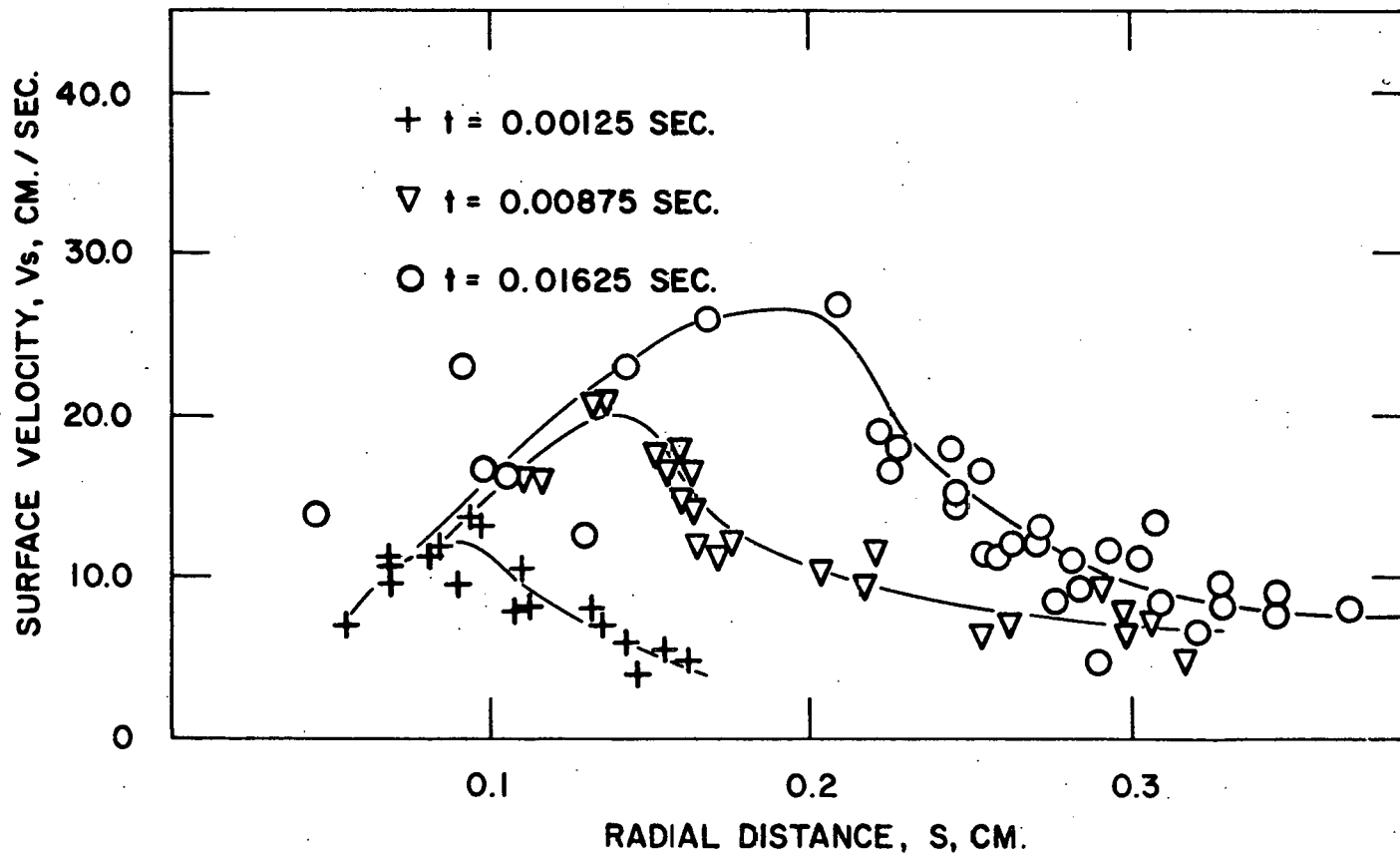
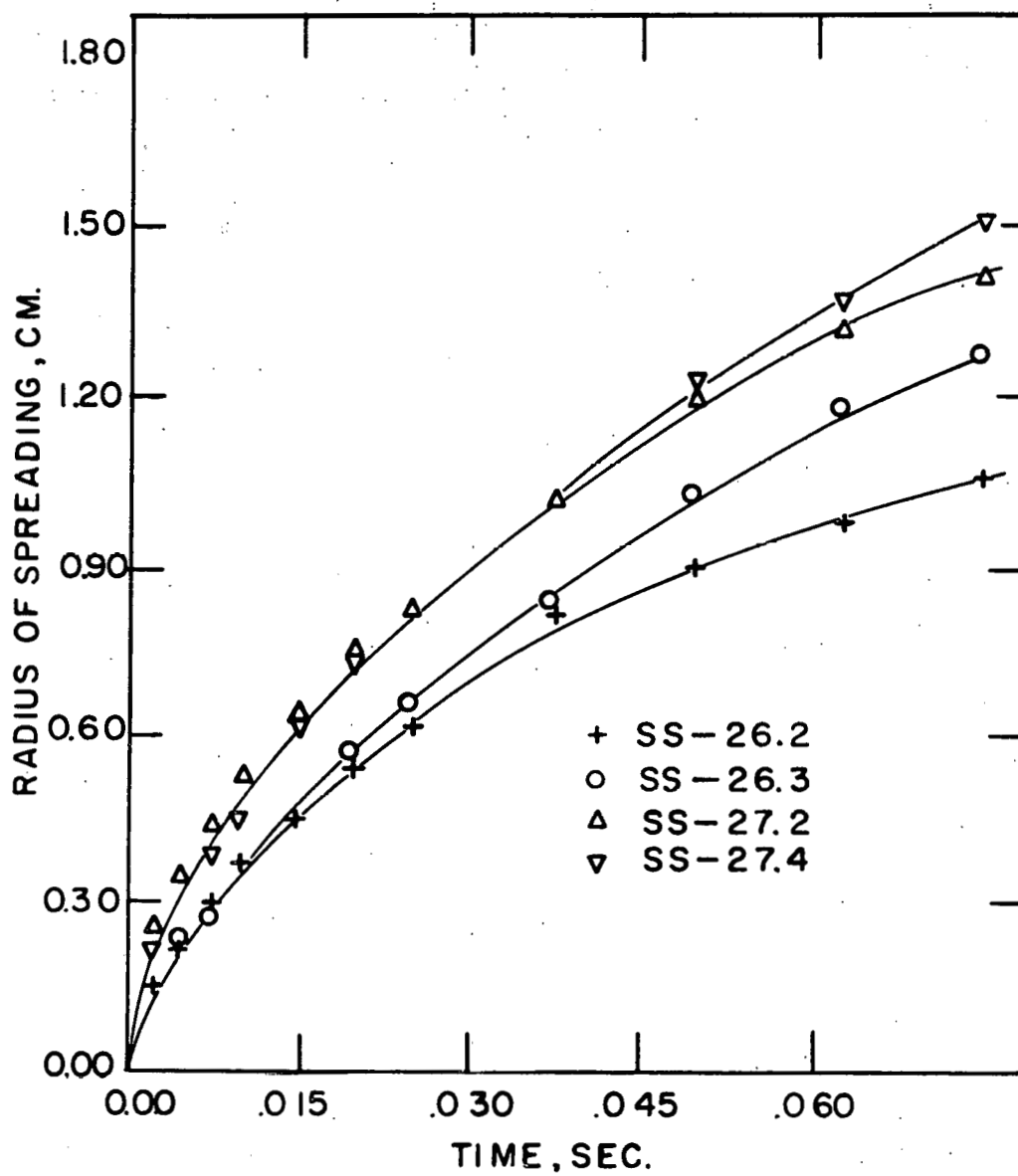Figure 23. Typical curves for interfacial velocity versus radial distance.

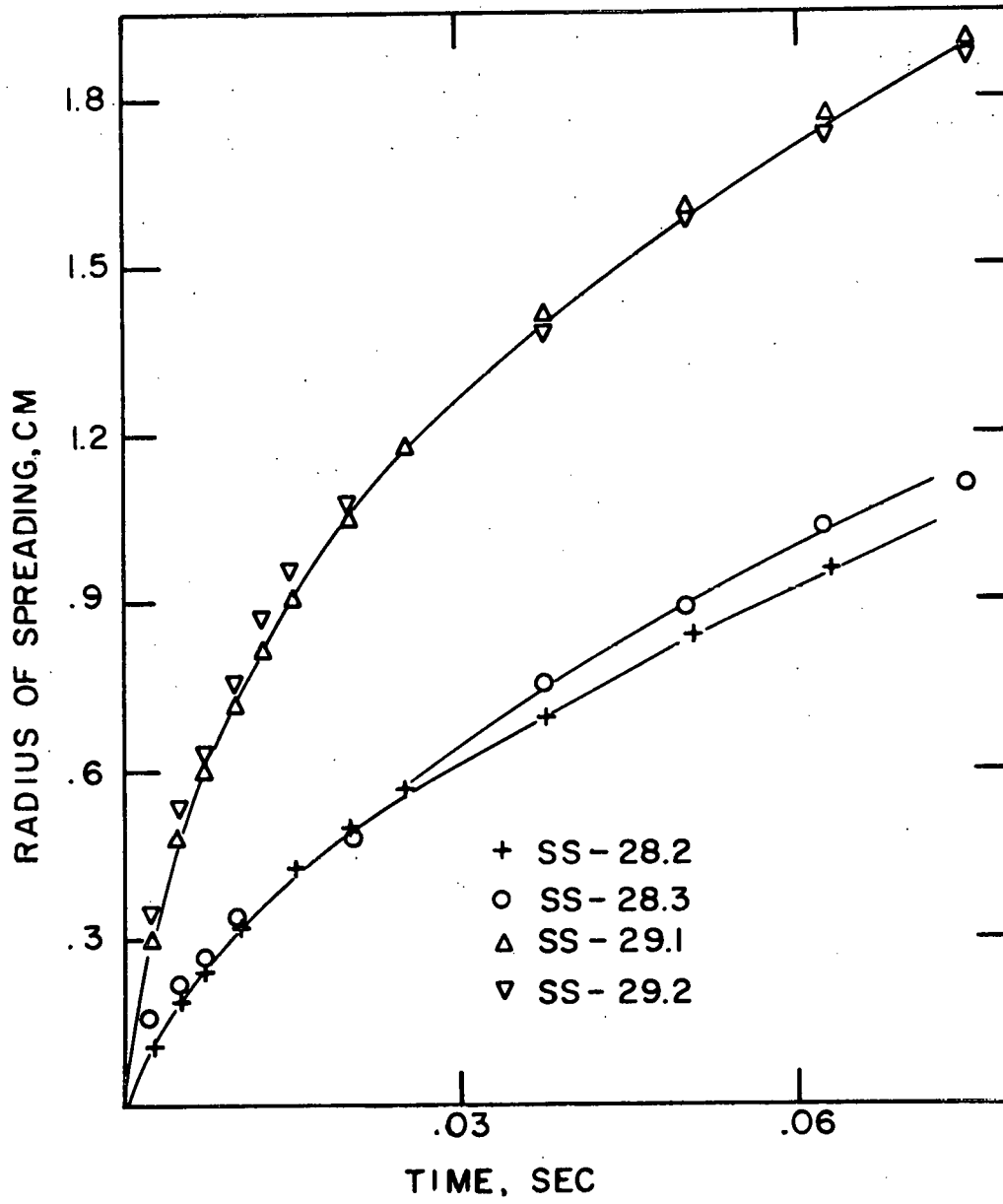Figure 24. Solute spreading for the negative-beta system.

Figure 25. Solute spreading for the positive-beta system.

Table 2. Experimental conditions that were imposed on a flat interface

Code	Volume of solute microliters	Solute concentration % cyclohexanol	Organic phase	σ at end of run
SS-26.2	0.1	10	Cyclohexane	
SS-26.3	0.2	10	Cyclohexane	42.1
SS-27.2	0.1	20	Cyclohexane	
SS-27.4	0.2	20	Cyclohexane	41.5
SS-28.2	0.1	10	CCl_4	
SS-28.3	0.2	10	CCl_4	43.3
SS-29.1	0.1	20	CCl_4	
SS-29.2	0.2	20	CCl_4	42.9

The graphs in Figures 24 and 25 show that the amount of solute used has little effect on the spreading rate, but the larger volume of solute will spread further and for a longer period of time. Initially the spreading is quite rapid but tapers off as time increases. This is probably due to the depletion of solute at larger values of radius from dissolution and increase in area proportional to s^2. The initial solute concentration has a greater effect on the rate of spreading than an increased volume of solute.

APPENDIX II

Droplet Data

This section contains some of the measurements made on dynamic and static drop profiles. All measurements were made from the projection of film on white paper. Four negative-beta and three positive-beta drops were filmed. The static droplet profiles were measured before each application of solute. The average σ and b values were used in the description of the static drop. The b and σ values were found from a two-parameter fit to each droplet profile. The last distinguishable point at the base of the drop was also measured so that droplet height and diameter could be used as boundary conditions. The data for static drops are given in Tables 3 and 4.

Table 3. Static droplet data

Label	Volume cm.^{3}	b cm.	σ dynes/ cm.	Height cm.	Base diameter cm.	System Organic	Initial apex pressure change, dynes/cm.^{2}
DD-13.1	.983	0.89	37.0	.525	1.37	Cyclo-hexane	63.0
DD-14.1	.67	1.85	42.9	.289	1.43	Cyclo-hexane	36.7
DD-15.1	.91	1.28	43.1	.414	1.40	Cyclo-hexane	53.2
DD-16.1	.97	1.20	41.8	.440	1.46	Cyclo-hexane	54.6
DD-17.1	.116	0.47	36.2	.403	.252	CCl_4	115.0
DD-18.1	.211	0.66	40.3	.458	.342	CCl_4	95.0
DD-19.1	.054	0.29	47.1	.360	.171	CCl_4	262.0

Table 4. Experimental conditions imposed on the static drops

Label	Volume of solute, microliters	Solute concentration % cyclohexanol	Corresponding spreading data
DD-13.2	0.1	10	SS-26.2
DD-13.3	0.2	10	SS-26.3
DD-13.4	0.1	10	SS-26.2
DD-14.2	0.1	20	SS-27.2
DD-14.3	0.2	20	SS-27.4
DD-14.4	0.2	20	SS-27.4
*DD-15.2	0.1	20	SS-27.2
DD-15.3	0.2	20	SS-27.3
DD-15.4	0.2	20	SS-27.3
DD-16.2	0.1	10	SS-26.2
DD-16.3	0.2	10	SS-26.3
DD-16.4	0.2	10	SS-26.3
DD-17.2	0.1	10	SS-28.2
DD-17.3	0.2	10	SS-28.3
DD-17.4	0.1	10	SS-28.2
*DD-18.2	0.1	20	SS-29.1
DD-18.3	0.2	20	SS-29.2
DD-18.4	0.1	20	SS-29.1
DD-19.2	0.1	10	SS-28.2
DD-19.3	0.2	10	SS-28.3
DD-19.4	0.1	10	SS-28.2

*Used for comparison to dynamic model

The apex movement for all the conditions in Table 4 are plotted in Figures 26 through 32. As would be expected from spreading data, each drop behaved the same for 0.1 and 0.2 microliters of solute. However, the concentration probably has an effect, although the quantity of data is insufficient to make such a conclusion. The movement of the apex is to some extent related to the initial apex pressure change, but a direct correlation is impossible since it is also influenced by such factors as viscosity, drop volume, curvature, and mass resistance to motion.
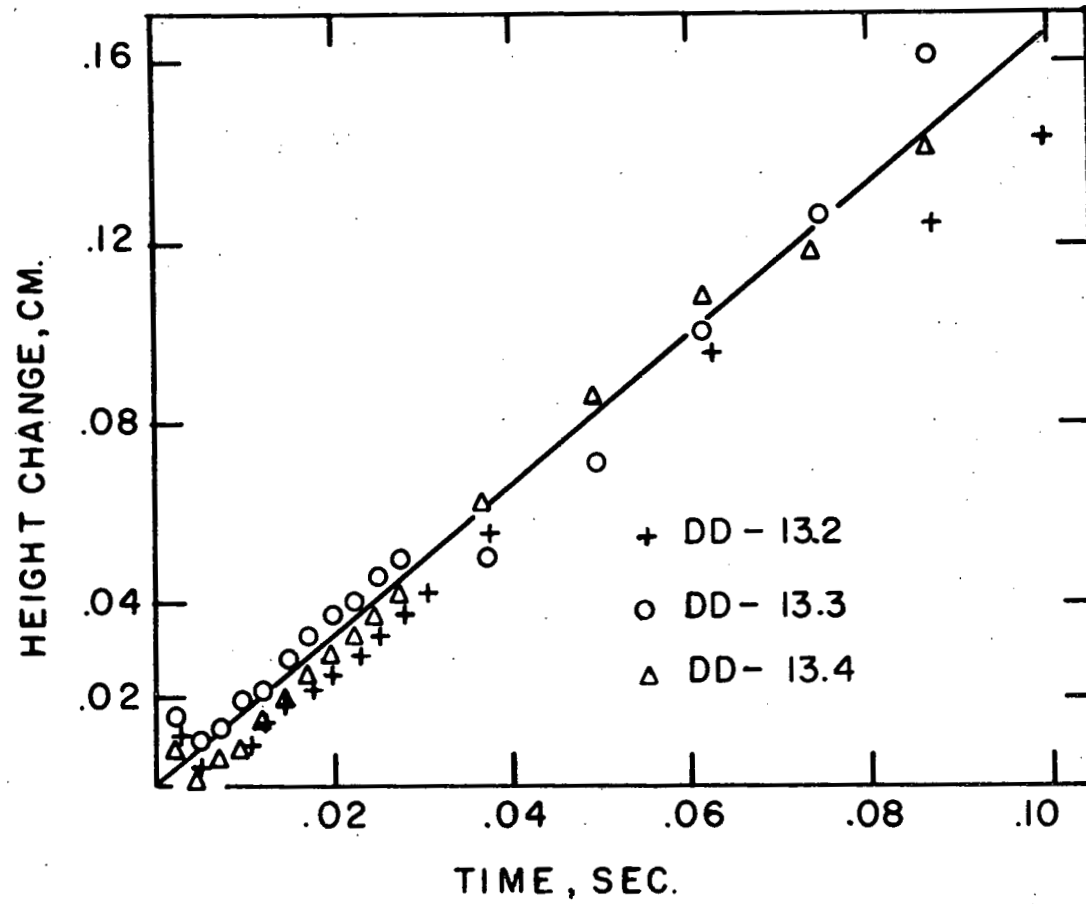
Figure 26.   Change of droplet height for negative-beta drop, DD-13.
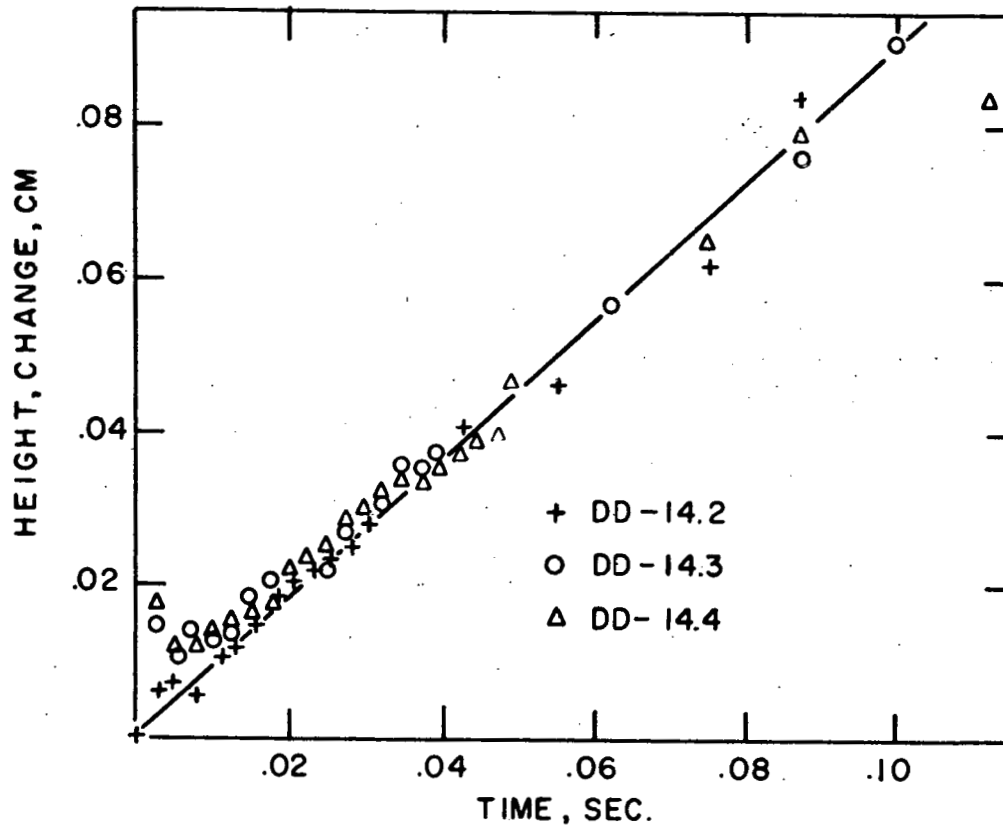
Figure 27. Change of droplet height for negative-beta drop, DD-14.
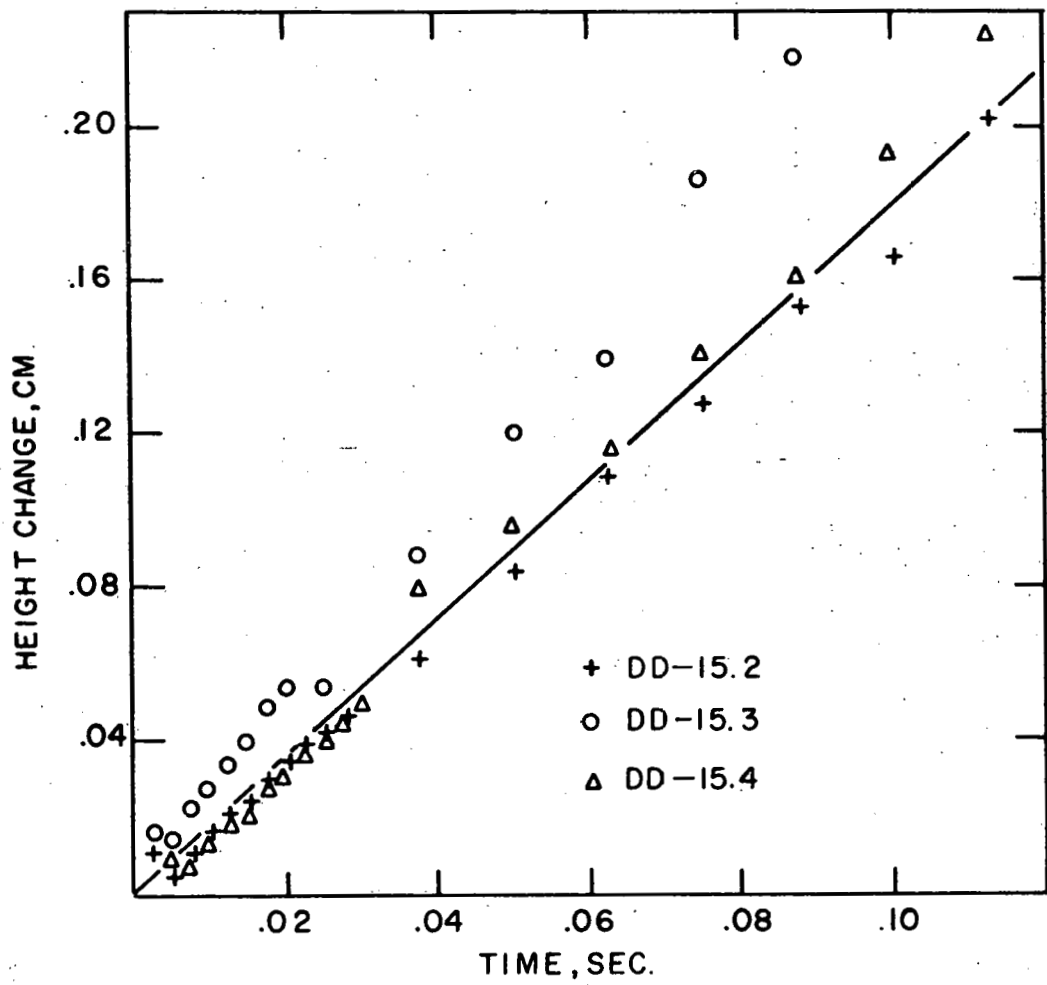
Figure 28.   Change of droplet height for negative-beta drop, DD-15.
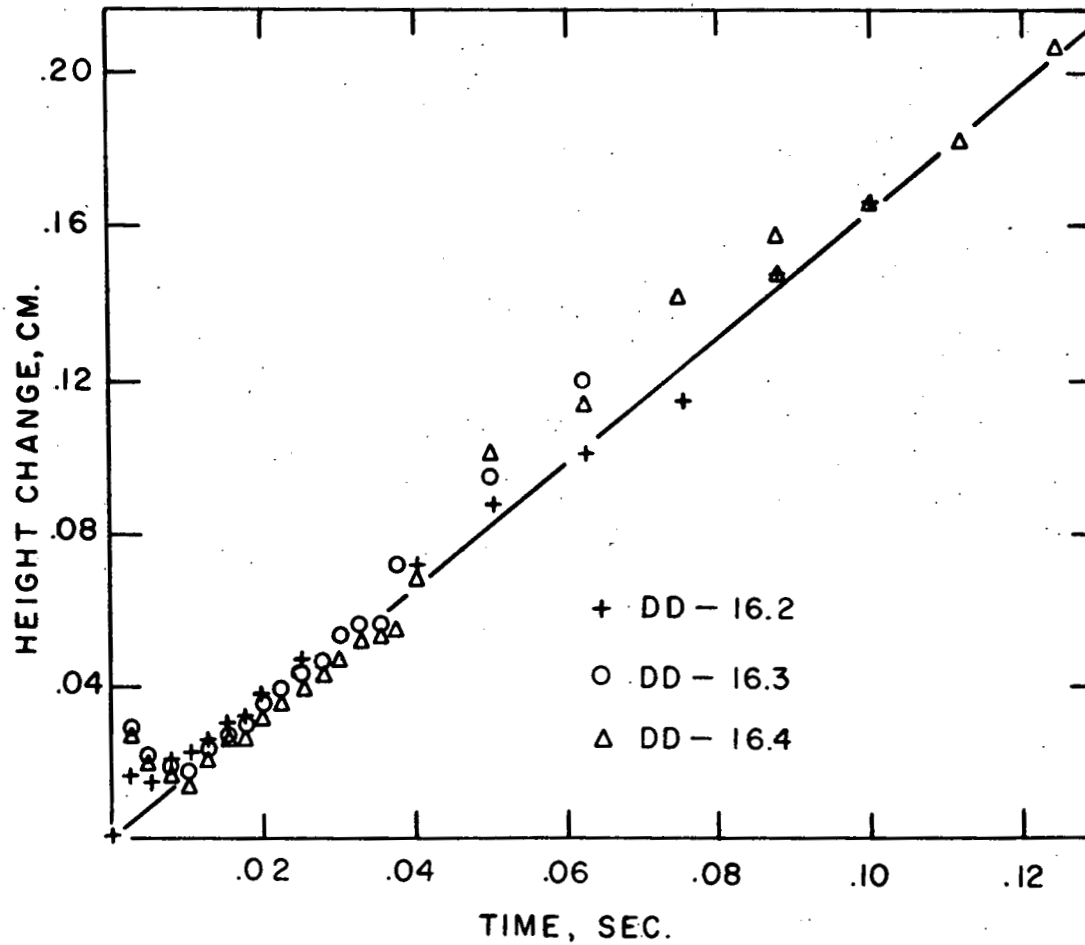
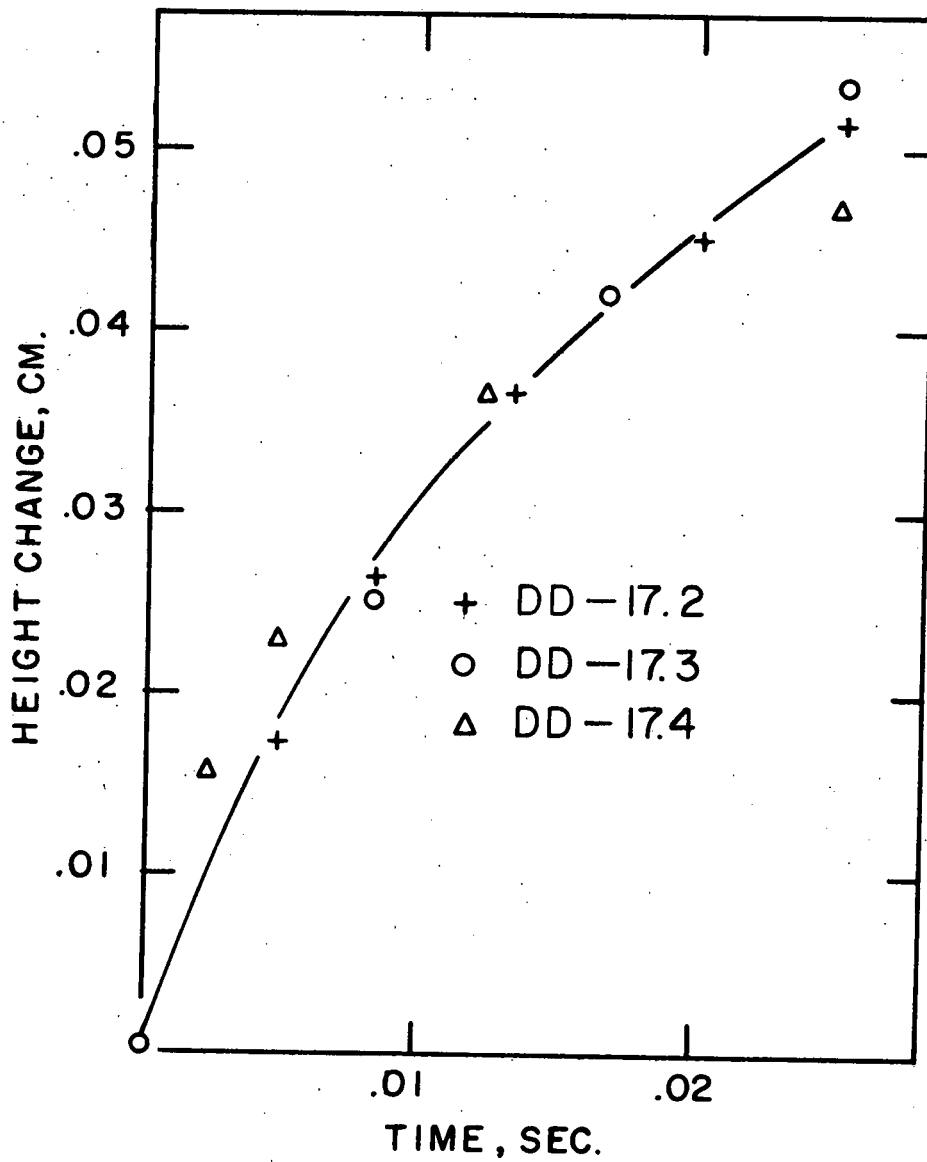Figure 29. Change of droplet height for negative-beta drop, DD-16.

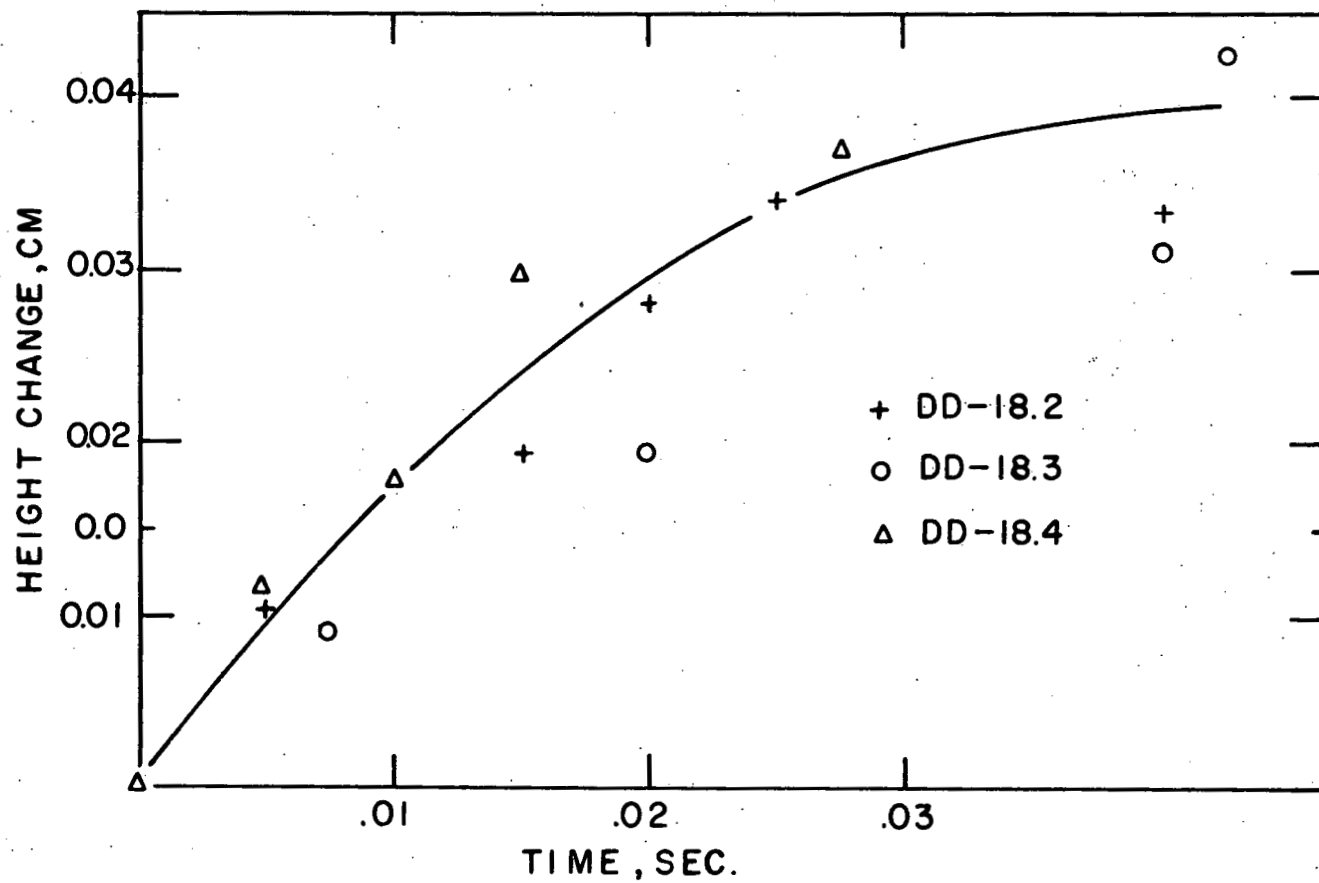Figure 30. Change of droplet height for positive-beta drop, DD-17.

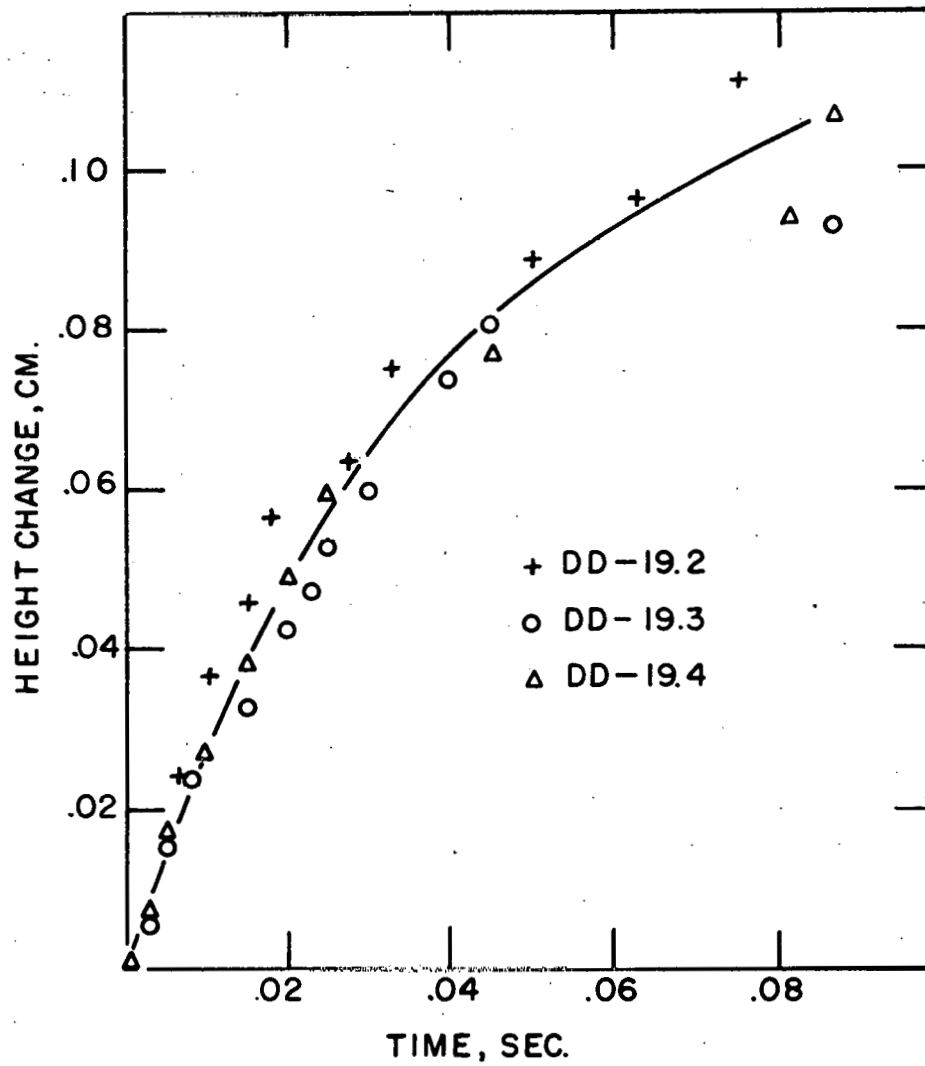Figure 31.   Change of droplet height for positive-beta drop, DD-18.

Figure 32. Change of droplet height for positive-beta drop, DD-19.